

FINAL TECHNICAL REPORT

Project Title: DEVELOPMENT AND DEPLOYMENT ASSESSMENT OF A MELT-DOWN PROOF MODULAR MICRO REACTOR (MDP-MMR)

Covering Period: October 1st, 2014 through September 30th, 2017

Date of Report: April 2, 2018

Recipient: North Carolina State University
P.O. Box 7909
Department of Nuclear Engineering
Raleigh, NC 27695-7909

Project Number: NEUP 14-6782

Principal Investigator: Ayman I. Hawari
(919) 515-4598
ayman.hawari@ncsu.edu

Collaborators: Francesco Venneri (Ultra-Safe Nuclear Corporation)
fvenneri@utrasafe-nuclear.com

Project Objective: The objective of this project is to perform feasibility assessment and technology gap analysis and establish a development roadmap for an innovative and highly compact Micro Modular Reactor (MMR) concept that integrates power production, power conversion and electricity generation in a single unit. The MMR is envisioned to use fully ceramic micro-encapsulated (FCM) fuel, a particularly robust form of TRISO fuel, and to be gas-cooled (e.g., He or CO₂) and capable of generating power in the range of 10 to 40 MW-thermal. It is designed to be absolutely melt-down proof (MDP) under all circumstances including complete loss of coolant scenarios with no possible release of radioactive material, to be factory produced, to have a cycle length of greater than 20 years, and to be highly proliferation resistant. In addition, it will be transportable, retrievable and suitable for use in remote areas. As such, the MDP-MMR will represent a versatile reactor concept that is suitable for use in various applications including electricity generation, process heat utilization and propulsion.

Background: An important difference at the point of operation between non-nuclear and nuclear power generators is the release of substantial amounts of decay heat after power production has ceased and the reactor has shut down. With the production of decay heat comes the possibility that a reactor core

may melt down during an accident that prevents the continued cooling of the core after shut down. The possibility of core melt down is increased in the event of a Station Black Out (SBO), when external and internal power to the reactor are not available to dissipate the decay heat. This problem is worsened by the high thermal power of typical reactors and compounded by the continuing push to design ever-higher power density cores in order to achieve better “economy of scale”. Newer, redundant safety systems – external to the reactor core – are routinely added to the new designs, leading to additional plant cost and complexity, and increasingly unappealing economic returns. It is estimated that nearly 30% of the overnight cost of a nuclear power plant is directly related to safety systems. Moreover, as demonstrated by the Fukushima events, the probability of a catastrophic accident may be extremely low, but the consequences are also extremely expensive.

In order to take advantage of the “economy of mass production” as introduced for most other power systems, such as gas-fired turbines, the problem of decay heat removal needs to be clearly resolved, with the assurance of no possibility of melt down, core damage and radioactivity release – ever – without relying on expensive external safety systems that may or may not be available when needed. In other words: the safety of the reactor should be inherent, absolute, and contained in the reactor itself. This project introduces a very compact reactor concept that integrates power production, power conversion and electricity generation within a single unit – the Micro Modular Reactor (MMR). The reactor is designed to be “melt-down proof” (MDP) under extreme circumstances, including complete loss of coolant, and is easily transportable and retrievable, and suitable for use with minimal site preparation and Balance of Plant requirements. The MDP-MMR is designed so that it has no chance of dispersing radioactive material. It is sealed with a lifetime of fuel loaded at the factory and inaccessible to the user/operator. It would be fully assembled at the factory, including a full complement of fuel, transported to the site of operation and started, with a small amount of pre-arranged, standardized preparation and construction work.

Initially, the MDP-MMR will be attractive for use in remote areas that are currently served by very expensive diesel generator produced power. However, it is possible to envision that the MMR, once the appropriate licensing framework is accomplished, will be suitable for large-scale deployment similar to gas-fired systems. Given the benefit of the much lower and more stable cost per unit energy produced by nuclear fuel compared to fossil fuels, it is also possible to envision that such reactors, when produced in large numbers, will be generating power at economically competitive prices.

The following major tasks were executed during the course of this project to analyze the technological and implementation aspects of the MDP-MMR.

1) Neutronic modeling of the MDP-MMR

During this project, A Monte Carlo (MCNP6) model of the MPD-MMR was developed to perform neutronic analysis. The model describes a cylindrical core composed of 4 fueled layers and 2 reflector layers. The layers are made of hexagonal graphite blocks that contain SiC compacts with UCO TRISO particles. The model uses geometrical and material symmetry to reduce complexity and computational execution demands. At this time, 656 burnable materials and 20 unburnable materials are included in the model. The fuel is enriched to 12% in U-235. The initiating fission source is distributed in the core in 63 locations and is represented by a Watt spectrum.

The core is composed of 37 assemblies. The control rod assembly and fuel rod assembly are hexagonal shape assemblies 30 cm in width. There are 48 and 54 fuel pins in the control rod assembly and the fuel assembly, respectively. The number of helium cooling channels are 18 and 19 in the control rod assembly and the fuel assembly, respectively. The diameter of helium cooling channel is 1.55 cm. The diameter of fuel pin is 2.17 cm. The diameter of the control rod is 8 cm. The control rod assembly and fuel rod assembly in reflector layer are exactly the same geometry with the fuel layer assemblies except for that there exists no fuel rods. The reserved emergency shutdown assembly, which is located in the center of the reactor core consists of pure graphite and one single control rod of 12 cm diameter. The fuel rod is made up of top and bottom graphite reflector 2.38 cm in height and middle fuel component 63.24 cm in height. The fuel is a mixture of UO_2 and UCO with a mole fraction of 1:1. In the fuel, the mole fraction of U:C:O is 2:1:3, thus the fuel can be written by short hand as U_2CO_3 . The fuel has 12% enrichment. The reactor is surrounded by the reactor vessel made of alloy A800H, reflector layer made of BeO and Graphite. The alloy A800H is a well-known iron base alloy with excellent corrosion resistance as well as strength at high temperatures.

In the MCNP model, the core is divided into four rings of assemblies. Each ring carries different symmetry. To reduce CPU time, the MCNP model takes advantage of the symmetry of the core. It is advantageous to divide the core into 6 high symmetry circular sectors. Each of the sectors is subjected to the same physics. In Figure 1, the area between the two red lines shows an example of the high symmetry core region. To support safety analysis needs, the MCNP model was used to calculate the power distribution in the core. This analysis was performed by evaluating the fission energy deposition in each fuel segment. It included 328 fuel pins, each divided into 5 different axial segments, with the two bottom fuel segments having the same temperature. In this case, a total of 1640 fuel segments are used in the MCNP calculation. Different combinations of F7 fission energy deposition tallies are calculated in the model assuming unburned clean conditions at the beginning of the power cycle. The results are given in Figure 2 below. the pin power distribution is largely affected by the radial power distribution. The innermost fuel pins generate the most fission energy.

The coolest fuel pins are those in assembly 301, 302 and 303. The fuel pins in assemblies 401 to 404 are of higher fission energy deposition because of the reflected neutrons from graphite and BeO surrounding the core.

In the depletion process, the reactor burns at a constant 10MWth power. There are a total of 70 burn up steps. Execution of the current model results in a value of excess reactivity of approximately 30,000 pcm. Figure 1 shows the MCNP model and Fig. 2 below shows results of the depletion analysis.

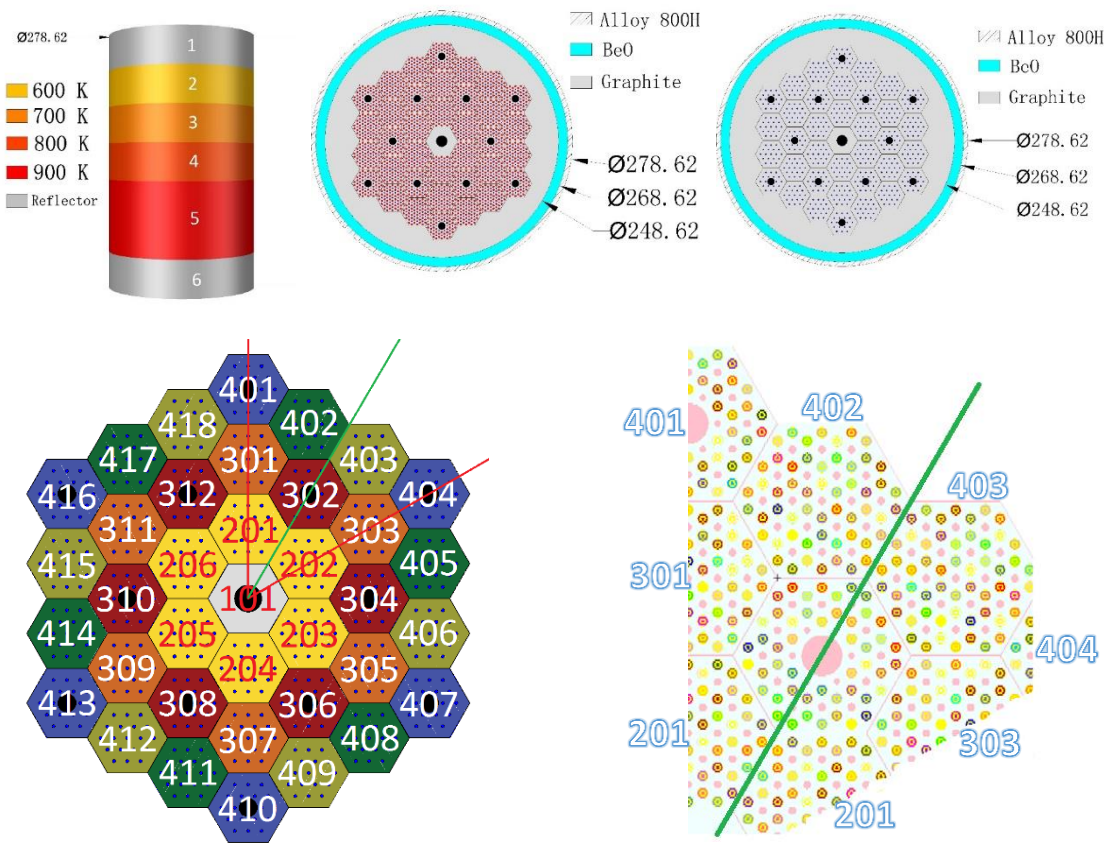


Fig. 1. The Monte Carlo (MCNP) model of the MDP-MMR core. The top sketches (left to right) show the core, the fueled layer and the reflector layer, respectively. The bottom sketches (left to right) show the symmetrical configuration of the core and the fuel in a layer.

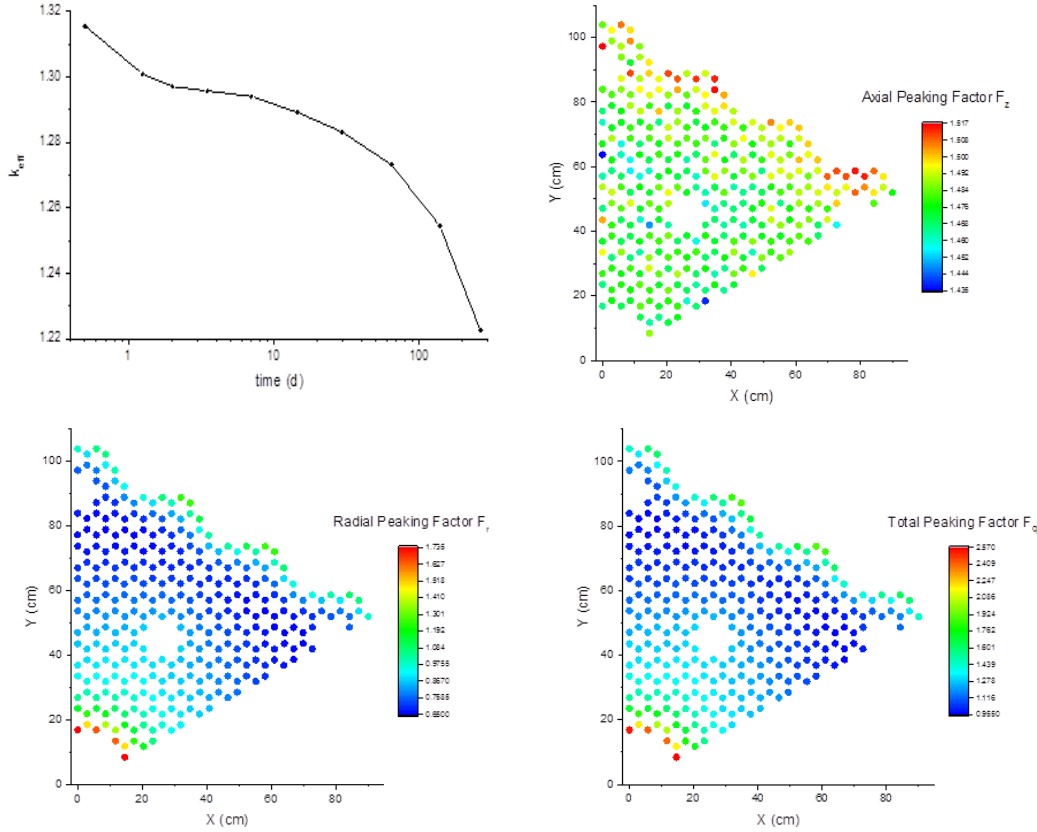


Fig. 2. The depletion data for the MDP-MMR core (top left). The power distribution for the MDP-MMR core (top right and bottom).

2) Neutron thermal scattering analysis for SiC and graphite

3C Silicon carbide (SiC) was evaluated by the LEIP group at NCSU with the AILD method. Ab-initio simulations of the 3C-SiC zinc blende crystal structure were performed using the VASP code. The Hellmann-Feynman forces calculated from these simulations were used in the PHONON code to determine the phonon DOS for each element in the system with the lattice dynamics method. Subsequently, the partial phonon DOS for C and Si in SiC were utilized to produce the TSL (File 7) 300, 400, 500, 600, 700, 800, 1000, and 1200 K for C(3C-SiC) and Si(3C-SiC) were generated in the incoherent approximation using the NJOY code. The coherent elastic cross section of 3C-SiC was evaluated by the generalized Debye-Waller matrix method using a modified LEAPR routine. The total scattering cross section of SiC at 300 K and inelastic cross section at different temperatures are shown in Fig. 3 below. The SiC TSL libraries, Si (3C-SiC) and C (3C-

SiC), represent new evaluations in ENDF/B-VIII that are included for the first time in the ENDF/B database.

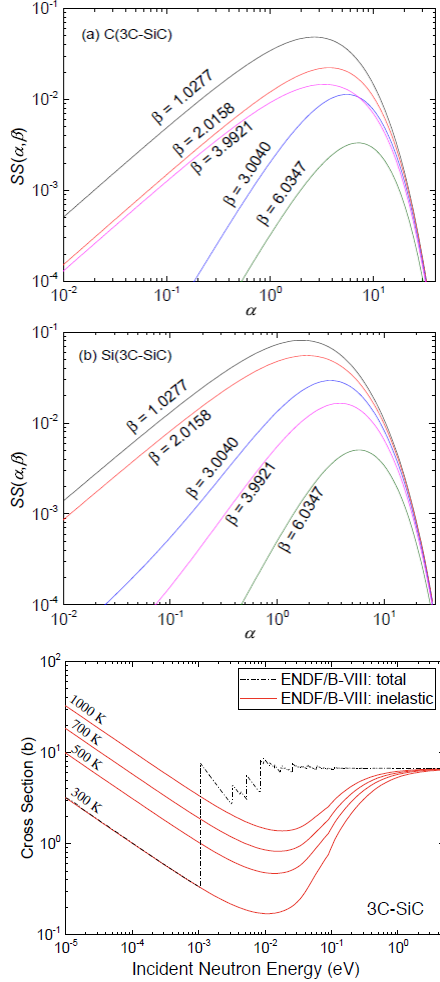


Fig. 3. The SiC TSL (top and center) at 300 K, and total (inelastic and elastic) thermal scattering cross section (bottom) at various temperatures.

Nuclear/reactor graphite was evaluated by using classical molecular dynamics (MD). It represents a multi-phase material composed of micro crystallites connect through a carbon binder matrix; consequently, this form of graphite is highly porous and has atomic vibrational behavior that differs significantly from crystalline graphite. Initially, an MD model of crystalline graphite was created and validated against measured thermodynamic properties. To capture the impact of porosity present in nuclear graphite, atoms were randomly removed from the crystalline structure. Subsequently, the system was evolved to generate time dependent velocities, from which the phonon DOS was calculated as the

Fourier transform of the velocity auto-correlation function. The TSL at 296, 400, 500, 600, 700, 800, 1000, 1200, 1600, and 2000 K were evaluated in the incoherent approximation using the LEAPR module of the NJOY code. The symmetric TSL at 296 K is shown below. Due to the similarities in crystalline structure, the coherent elastic scattering behavior of crystalline graphite may be assumed to be representative of nuclear/reactor graphite. Total scattering cross sections, processed with THERMR, are shown in Fig. 4 below. The evaluated ENDF/B-VIII total cross section is compared to ENDF/B-VII.1 at 296 K. Moreover, the ENDF/B-VIII inelastic cross sections are compared to cross section measurements of nuclear/reactor graphite for increasing temperature. The ENDF/B-VII.1 is the traditionally available TSL library. The presented ENDF/B-VIII inelastic scattering cross section for nuclear/reactor graphite shows improved agreement with measurement. Nuclear/reactor graphite represents a new TSL evaluation that is included for the first time in the ENDF/B database.

Access to the SiC and graphite libraries can be found in the “Thermal Neutron Scattering Sublibrary” at <http://www.nndc.bnl.gov/endf/b8.0/download.html> .

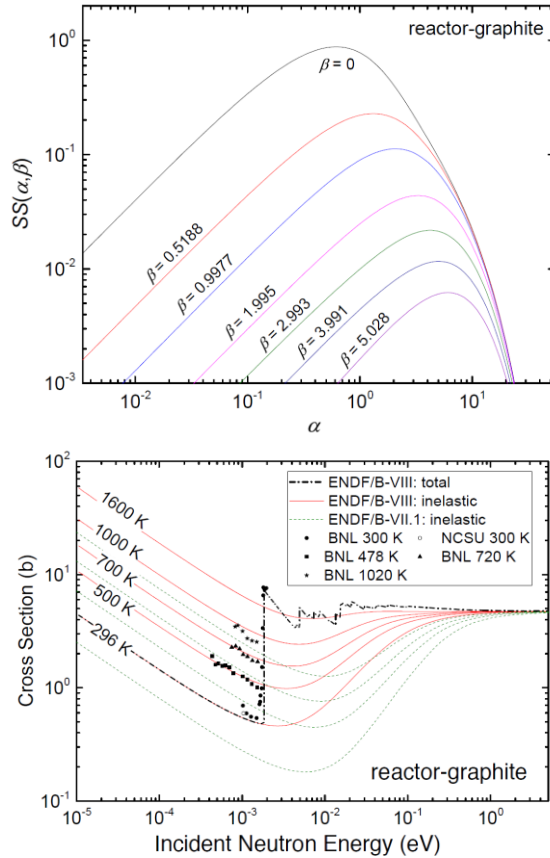


Fig. 4. The nuclear/reactor graphite scattering law at 296 K (top) and the thermal scattering cross sections (bottom) at various temperatures.

3) Safety analysis

Thermal hydraulic analysis tool is essential for safety analysis. For level 1 PSA, we need to know the reactor core and fuel response on various incidents with reasonable accuracy. There are already many T/H tools available. However, they need detailed description of reactor core, take relatively long execution time, and has limitations on handling multiple heterogeneity of MMR. We decide to develop new computer programs for this study. The developed computer programs should be fast enough to handle very long term response of several weeks due to decay heat as well as fast transient such as prompt reactivity excursion in sub milliseconds. The methodology should include all important phenomena of the gas cooled reactor with reasonable accuracy.

Thermal analysis model

MMR is a gas cooled reactor composed of conducting disk blocks which have a large number of fuel compacts and coolant holes at the core region. The core region is surrounded by annular reflector with coolant riser channels. The reflector region is enclosed by a metallic pressure vessel. During the normal operation, heat is removed by coolant channels in core region. In accidental situation, latent and decay heat of reactor core is dissipated by radiation heat transfer on the surface of the reactor vessel. Detailed description of the geometry is practically impossible due to multiply heterogeneous geometry of TRISO particles and coolant holes. It is not necessary at this stage of research to do detailed analysis. MMR geometry is locally periodic in various scales. An FCM compact is cluster of identical spherical TRISO particles. Core region is a repetition of hexagonal unit cells. The periodic structure problem can be solved using the generalized perturbation method proposed by Bensoussan [Bensoussan, 1978] Stainsby [Stainsby, 2009] and Allaire et al [Allaire, 2013] have applied the method to diffusion problem such as heat conduction problem or neutron diffusion problem successfully.

Figure 5 displays a view of temperature distribution in the generalized perturbation theory. Local temperature is sum of the global, the meso scale, and the TRISO scale temperatures which is varying periodically depending on the scale of view.

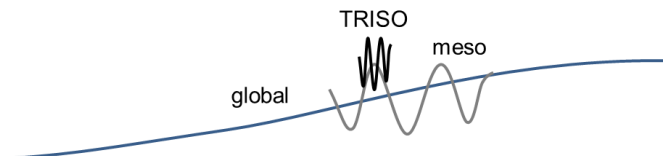


Figure 5. Temperature distribution

We adopted “homogenization” method for the diffusion problems as developed by Stainsby for the pebble-bed and prismatic block gas cooled reactors. Stainsby has verified its validity by comparing the developed homogenization procedure with detailed method for various transient cases as well as steady state cases. We developed a computer code system consist of “Global” – “Meso” – “TRISO” scale models for the MMR analysis. Figure 6 displays the thermal analysis modules developed in this study. Each module is executed until convergence is achieved.

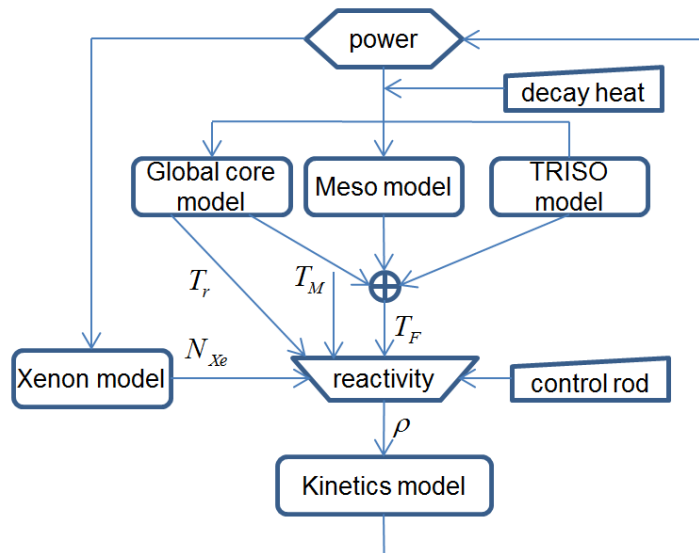


Figure 6. Reactor core analysis model

Global model

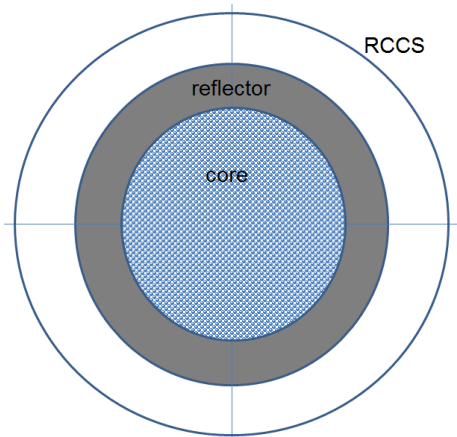


Figure 7. Porous core model

The core is modeled as a porous cylindrical disk by averaging axial direction of the core as shown in Figure 7. In the porous model, generated heat is removed at the same location as well as transferred to neighboring location during normal operation. Heat is produced in the core region, transferred through the graphite blocks, and removed through coolant holes in the core region. When the helium circulator is stopped, the heat is transferred at the outer surface of the reactor vessel, then the heat is removed through radiation heat transfer to the RCCS(Reactor Cavity Cooling System). The temperature, T , is calculated by following heat balance equation in a global porous disk model

$$\rho C_p \frac{\partial T}{\partial t} = \frac{\partial}{r \partial r} \left(kr \frac{\partial T}{\partial r} \right) + q(r, t) - hA(T - T_B) .$$

Boundary condition at the outer surface is written as follows

$$k \frac{\partial T}{\partial r} = \varepsilon \sigma A (T^4 - T_c^4) ,$$

where, t is the time and r is the radial distance from the center of core. ρC_p is the heat capacity, k is the effective conductivity of core region, q is the heat generation rate. hA is the heat transfer rate coefficient at the coolant holes and T_B is the axial averaged coolant bulk temperature. $\varepsilon \sigma A$ is the radiation heat transfer coefficient at the surface of reactor pressure vessel. T_c is the RCCS surface temperature.

Effective conductivity of porous fuel region is obtained by 3-zone Maxwell-Eucken formula averaging the core disk matrix conductivity, the helium coolant conductivity, and the effective compact thermal conductivity.

$$k_{eff} = k_m \left[1 - \frac{2[\alpha_1(k_m - k_1)(k_m + k_2) + \alpha_2(k_m - k_2)(k_m + k_1)]}{(k_m + k_1)(k_m + k_2) + \alpha_1(k_m - k_1)(k_m + k_2) + \alpha_2(k_m - k_2)(k_m + k_1)} \right]$$

where k_1 , k_2 and k_m are the conductivities of the FCM compact, and the helium, and the core disk matrix, respectively. α_1 and α_2 are the volume fraction of the FCM compact, and the coolant hole, respectively.

The effective conductivity of a compact is obtained by solving the spherical symmetric TRISO heat conduction problem with compact matrix.[Stansby, 2009. App. C] The result is the TRISO particle conductivity. The effective conductivity of an FCM compact is computed by 2-zone Maxwell-Eucken formula;

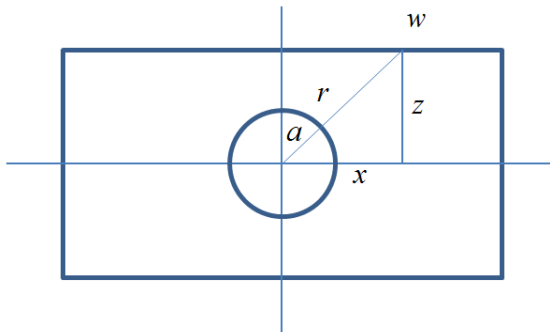


Figure 8. Effective conductivity of reflector region

Effective conductivity at the reflector region can be calculated by considering temperature field near a cylinder, which is coolant riser, as shown in Figure 8. The result is as follows

$$k_{eff} = \left[1 - \left(\frac{k_m - k_c}{k_m + k_c} \right) a^2 \frac{\arctan w/z}{wz} \right] k_m$$

where, a is the radius of riser channel. w is the half of the distance between riser. z is the half thickness of reflector zone. k_m and k_c are the conductivities of the graphite matrix and the coolant. Effective heat capacity is obtained by volume weighting method.

The temperature at an interesting location should be added by those obtained from the associated meso scale and TRISO scale model to the global model value.

Meso scale model

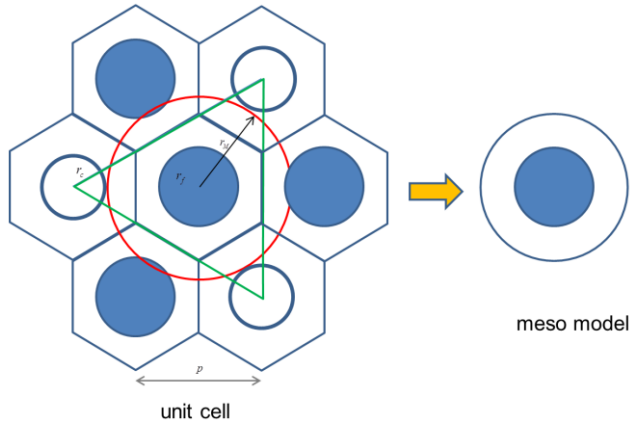
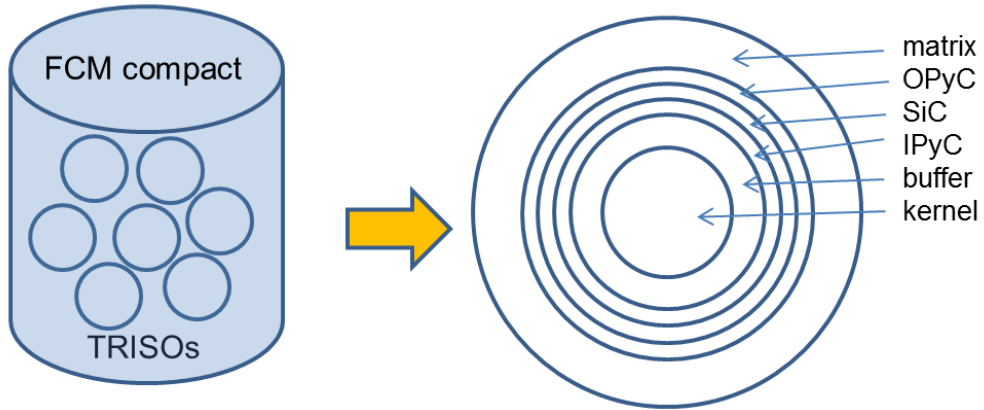


Figure 9. Meso scale model

The meso scale model describes the periodic perturbation from the smooth global temperature variation. Meso scale model is a unit cell conduction problem transformed to cylindrical model as shown at Figure 9. Fuel and graphite area is conserved between the meso scale model and the actual geometry. An adiabatic boundary condition and the net zero heat generation condition should be applied to obtain the temperature perturbation over the smooth global model temperature. Effective conductivity of fuel compact is the same value used in the global model. Convection heat transfer model requires the coolant channel surface temperature, Stainsby has introduced “super meso scale model” in which coolant hole is at the center of circle and fuel is distributed at periphery of the circle. The coolant hole temperature is added to the global model temperature to get the coolant channel surface temperature which determines the heat transfer coefficient. In this study, we are using simple heat transfer model assuming a fixed heat transfer coefficient. We omitted the “super meso scale model” in this study.

TRISO scale model**Figure 10. TRISO scale model**

The TRISO scale model (Fig. 10) describes periodic perturbation over the meso scale model temperature variation. A spherical unit cell conduction problem of TRISO particle surrounded by compact matrix material with adiabatic boundary condition and the net zero heat generation conditions are solved. Temperatures required to calculate material properties, are estimated by summing up the global temperature, the meso scale model temperature, and the TRISO model temperatures. Thickness of matrix region is calculated to keep the real matrix volume per TRISO.

$$PF = \frac{r_{OPyC}^3}{R^3} ,$$

where PF is the packing fraction, R and r_{OPyC} are the radius of TRISO scale model and OPyC, respectively. Temperature at the kernel region determines the Doppler effect.

Point kinetics model

Time dependent fission power is determined by following six-group point kinetics equation.

$$\frac{dN}{dt} = \frac{\rho(t) - \beta}{\Lambda} N + \sum_i \lambda_i C_i$$

$$\frac{dC_i}{dt} = \frac{\beta_i}{\Lambda} N - \lambda_i C_i$$

where, N is the neutron (or fission power) density, C_i is the number density of the delayed neutron precursor group i. ρ is the reactivity. β is total delayed neutron yield fraction. β_i and λ_i are the delayed neutron yield fraction, and the decay constant of group i.

The reactivity model is expressed as following.

$$\rho(t) = \alpha_F (T_F - T_F^0) + \alpha_M (T_M - T_M^0) + \alpha_R (T_R - T_R^0) + \alpha_{xe} \left(1 - \frac{N_{xe}}{N_{xe}^{eq}} \right) + \rho_{ext}$$

where, T_F , T_M , and T_R are the kernel, the moderator, and the reflector temperatures, respectively. Superscript “0” is used for respective reference temperatures. N_{xe} is the xenon number density and super script “eq” denotes the value at the full power equilibrium. α_F , α_M , α_R , and α_{xe} are the fuel temperature, the moderator temperature, the reflector temperature, and the xenon number density feedback coefficients, respectively. Finally ρ_{ext} is the external reactivity such as the reactivity introduced by control rod movement.

The fuel kernel temperature, which is used for Doppler feedback, is obtained by adding the core average temperature from global model, the compact region average temperature from the meso scale model, and the kernel region average temperature from the TRISO model. Moderator and reflector temperatures are obtained from the global model.

Decay heat model

After reactor shutdown, the fission power due to delayed neutron, the decay heat due to fission products, and the decay heat due to decay of actinides are the heat sources. Fission power is computed by the delayed neutron equation and decay heat is calculated by previous power history. Decay heat of actinides is much smaller than that of fission product. Decay heat is modeled by 23 group structure proposed by ANS.[ANS-1994] This structure is useful to model decay heat reflecting the power history as well as maintaining steady state at non-disturbed reactor.

$$P_d(t) = \int_{-T}^t P(t') f(t-t') dt'$$

$$f(t) = \sum_i \alpha_i e^{-\lambda_i t}$$

where P_d is the fission product decay heat. P is the power. α_i and λ_i is the fraction and decay constant of the fission product heat group i . T is the reactor operation time.

Xenon transient model

Point xenon transient equation is solved to model the long term contribution of xenon to the reactor criticality.

$$\frac{dI}{dt} = -\lambda_I I + \eta_I \Sigma_f \phi$$

$$\frac{dX}{dt} = -\lambda_x X - \sigma_x \phi X + \lambda_I I + \eta_x \Sigma_f \phi$$

I and X is the number density of I-135 and Xe-135 respectively. η_I and η_x are the I-135 and Xe-135 yield fractions per fission. λ_I and λ_x are the decay constants. $\Sigma_f \phi$ is the fission reaction rate. $\sigma_x \phi$ is the microscopic capture cross section of Xe-135 multiplied by the flux.

Time dependent calculation

In a gas cooled reactor transient calculation, the time constants of point kinetics, conduction, and xenon transient are widely varying from sub-milliseconds to few hours.

We adopted a kind of Runge-Kutta method TR-BDF2[Bank, 1985] which has capability of varying time step size with given desired accuracy.

Thermal Analysis of MMR

For current design, MMR produces 40 MWth from 20% enriched uranium of 3.44 ton in total. Specific power per unit mass of uranium is 11.6 kW/kg.

TRISO scale model

Thermal conductivity of materials are varying with temperature and irradiation. We adopt median values at around 1000K which is typical operation temperature at full power. As displayed at Table 1, thermal property of TRISO particle is adopted from Stainsby's report [Stainsby, 2009. Table 2.4.1]

Table 1. TRISO material property

Zone	radius (m)	conductivity (W/K/m)	density (kg/m ³)	heat capacity (J/kg/K)
Kernel	400	3.7	10000	500
Buffer	470	0.5	1000	2000
IPyC	505	4	2000	1900
SiC	540	16	3200	1200
OPyC	560	4	2000	1900
matrix	P.F. 40%	16	3200	1200

Weight of kernel in TRISO particle of 800 m is 2.78 mg. Nominal power density in the compact region is 23 MW/m³ which corresponds to 40 MW MMR. Figure 11 displays the temperature distributions in a TRISO particle with zero temperature boundary condition and the TRISO scale

model with adiabatic boundary condition. Upper curve in Figure 7 displays temperature of the zero BC case, the temperature rise from boundary is 4.2K. TRISO scale model temperature is shifted, 1.3K, almost parallel from that of zero temperature boundary condition. At outer region, temperature slope is linear in zero BC and that of TRISO scale model is zero.

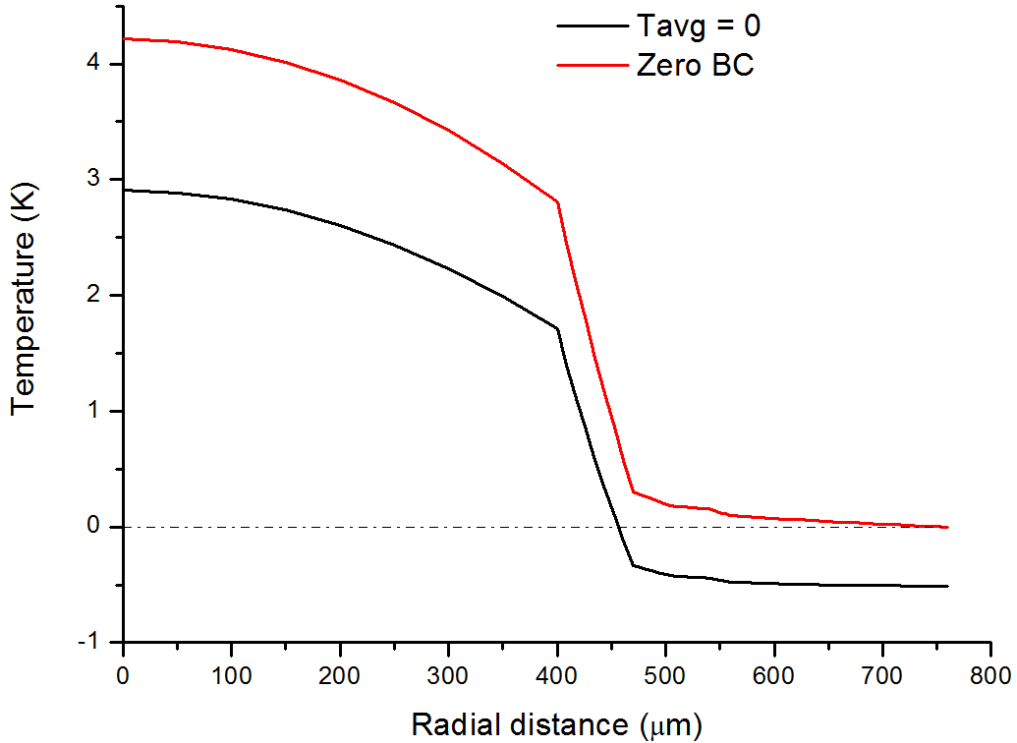


Figure 11. TRISO scale temperature distribution

Meso scale model

Meso scale model is an equivalent unit cell model surrounding the fuel compact. Equivalent conductivity of TRISO particle can be obtained by considering heat flux in a spherical particle as described by Stainsby. Equivalent conductivity of fuel compact is calculated by mixing the particle with matrix according to the Maxwell-Euken formula. For MMR TRISO, the effective conductivity of particle and compact are 3.8 W/K/m and 10.2 W/K/m, respectively. Effective heat capacity is 3.84 MJ/m³/K.

Figure 12 displays temperature distribution of meso scale model. Zero BC case shows that the center temperature is 46K higher than boundary temperature. Center temperature in a compact is 29K higher than smooth global temperature as calculated by adiabatic boundary meso scale model. Average temperature in the fuel region is added to the kernel temperature of TRISO scale and the core region average temperature of global model for Doppler feedback. We notice that the kernel peak temperature is 31.2K higher than the core temperature of global model.

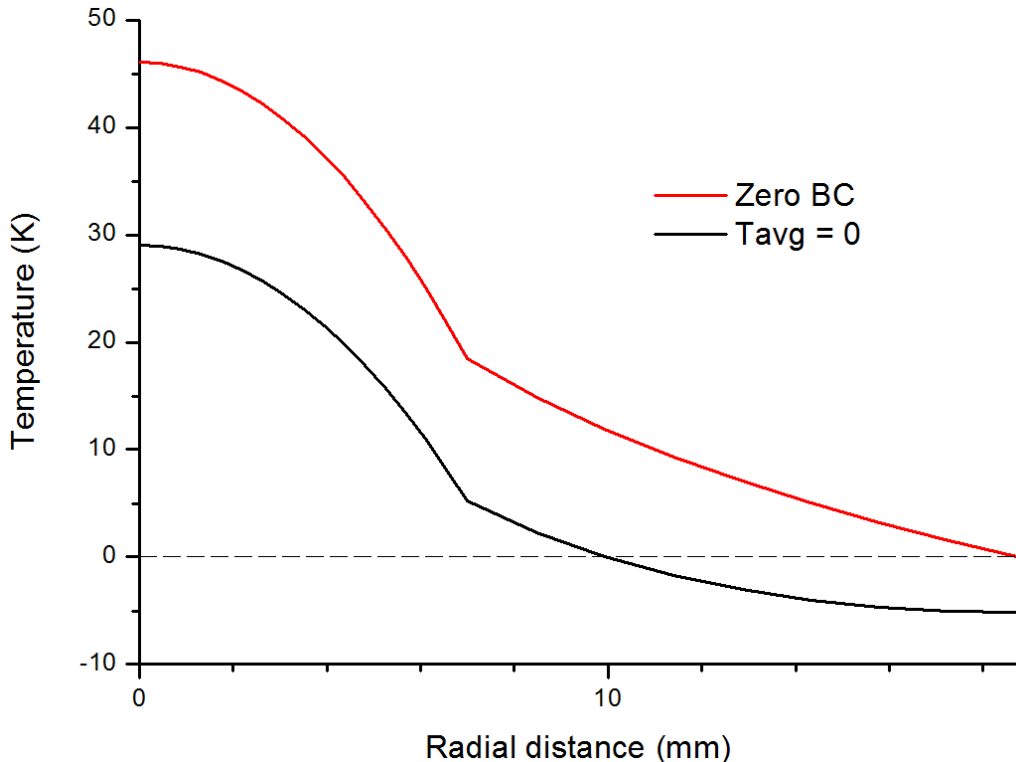


Figure 12. FCM compact temperature distribution in meso scale model

Global model

Effective conductivity of core region can be calculated by 3-zone Maxwell-Eucken formula. Conductivities of graphite and helium are 30 W/K/m and 0.35 W/K/m, respectively. [Stainsby, 2009] Effective conductivity of an FCM compact is 10.2 W/K/m as used in the meso scale model. Current unit cell geometry results effective global conductivity 25.1 W/K/m. Heat capacity can be calculated by volume weighting. The effective heat capacity of disk region is 3.0 MJ/m³/K. Fraction of fuel compact in core region is 0.278. For thermal analysis, heat transfer area and heat transfer coefficient is important quantity. However, we can adjust the total heat transfer area by core design and the heat transfer coefficient by varying blower speed and system pressure. Average power density at core region is obtained by 6.37 MW/m³. In this stage of study, we adjust heat transfer coefficient to give a target surface temperature rise from bulk coolant temperature. The heat transfer coefficient is 6.3 MW/m³/K for target surface temperature rise of 100K. In reflector region, we adopted the nominal properties of graphite, 30 W/K/m and 2.9 MJ/m³/K. Surface temperature of RCCS is set to 400K and the emissivity is assumed as 0.7.

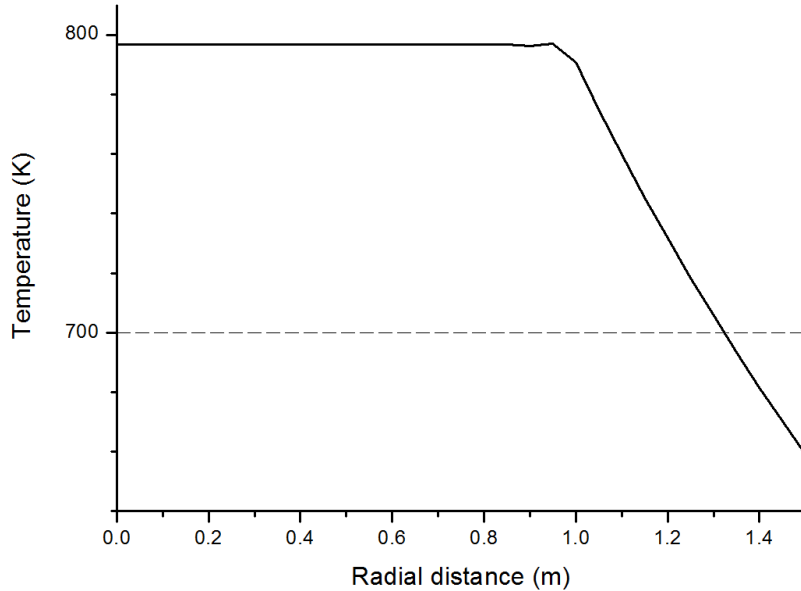
**Figure 13. Core temperature distribution**

Figure 13 displays steady state temperature distribution of core. During normal operation, the temperature in core region is almost flat since most of the generated heat is removed through helium coolant channels. Part of the generated heat is removed through radiation heat transfer at the surface of the reactor.

Transient properties

For safety analysis, it is important to use proper reactivity coefficients which is varying during core depletion. However, reliable MMR feedback data are not available until now. We adopted typical values from one of the HTGR analysis for this study [CKJo, 2017]. Table 2 shows the feedback coefficients used in this study. Fuel temperature (Doppler) feedback coefficient is defined as unit variation in the kernel temperature. Moderator temperature coefficient is based on the core region temperature of the global model. Xenon coefficient is obtained by criticality calculation by setting the xenon number density to zero from the equilibrium concentration. Xenon worth of a HTGR is much smaller than that of LWR due to hard neutron spectrum.

Table 2. Feedback coefficients

Parameter	value	unit
Fuel temperature(α_F)	-3.993	pcm/K
Moderator temperature(α_M)	-1.794	pcm/K
Reflector temperature(α_R)	2.002	pcm/K
Xenon(α_{Xe})	800	pcm

Table 3 shows the point kinetics parameters. Mean neutron life time, which is strongly dependent on neutron spectrum, is obtained by solving the multi-group neutron transport equation. The delayed neutron parameters are the weighted average of U-235, U-238, and Pu-239 fission rate. These values are obtained during core depletion calculation. We adopted a typical value for HTGR problem.

Table 3. Point kinetics parameters

Parameter	value	unit
mean neutron life time(Λ)	9.62E-04	sec
effective delayed neutron fraction(β_{eff})	5.09E-03	-
Six group parameters	λ_i	β_i / β_{eff}
group 1	0.0124	0.03307
group 2	0.305	0.21901
group 3	0.111	0.19594
group 4	0.301	0.39496
group 5	1.14	0.11504
group 6	3.01	0.04199

Table 4 shows the xenon parameters for xenon transient.

Table 4. Xenon transient parameters

Parameter	value	unit
Fission rate ($\Sigma_f \phi_0$)	1.70E-13	#/cm ³ /s
Capture rate per Xe-135 atom($\sigma_x \phi_0$)	2.76E-05	10 ⁻²⁴ /cm ³ /s
I-135 yield per fission (η_I)	0.064	-
Xe-135 yield per fission (η_{Xe})	0.0025	-

Decay heat model parameter is dependent on core burnup. At this stage, we adopt ANS recommendation for LWR U-235 thermal fission [ANS-1994].

Loss of cooling without trip

Loss of cooling is an extreme accident in a light water reactor that may result in fuel melting without an emergency core cooling system. In a gas cooled reactor, the conduction heat transfer through the graphite block will mitigate consequences by removing the residual heat and the decay heat by the radiation heat transfer at the pressure vessel surface. To avoid the fuel melting, the radiation heat transfer area should be large enough to dissipate the decay heat before

reaching melt temperature. We analyzed the consequence of sudden loss of cooling by setting the heat transfer coefficient zero at full power steady state condition. Figure 14 displays the fuel and reflector temperatures after complete loss of cooling and no control rod scram. Fuel temperature increases due to loss of cooling. Increase of fuel temperature introduces Doppler temperature feedback. Heat is conducted to the graphite blocks. At the reactor vessel surface, the heat is transferred to the RCCS by the radiation heat transfer. As displayed on Figure 14, the fuel temperature peaks at 14 hours on 1142K. Fuel temperature is decreasing after the peak due to conduction to the reflector region. However, further temperature decrease will introduce re-criticality at low power. Net reactivity of core is displayed on Figure 15. Net reactivity is decreasing until 14 hours. Then the reactivity is increasing to zero until 33.4 hours on when the reactor power is increasing. The positive reactive is inducing the power production to increase the fuel temperature. This behavior is a kind of cycling with damped oscillation until equilibrium is achieved if sufficient negative reactivity by control rod is provided. Figure 14 shows that the equilibrium fuel temperature is at 1299K.

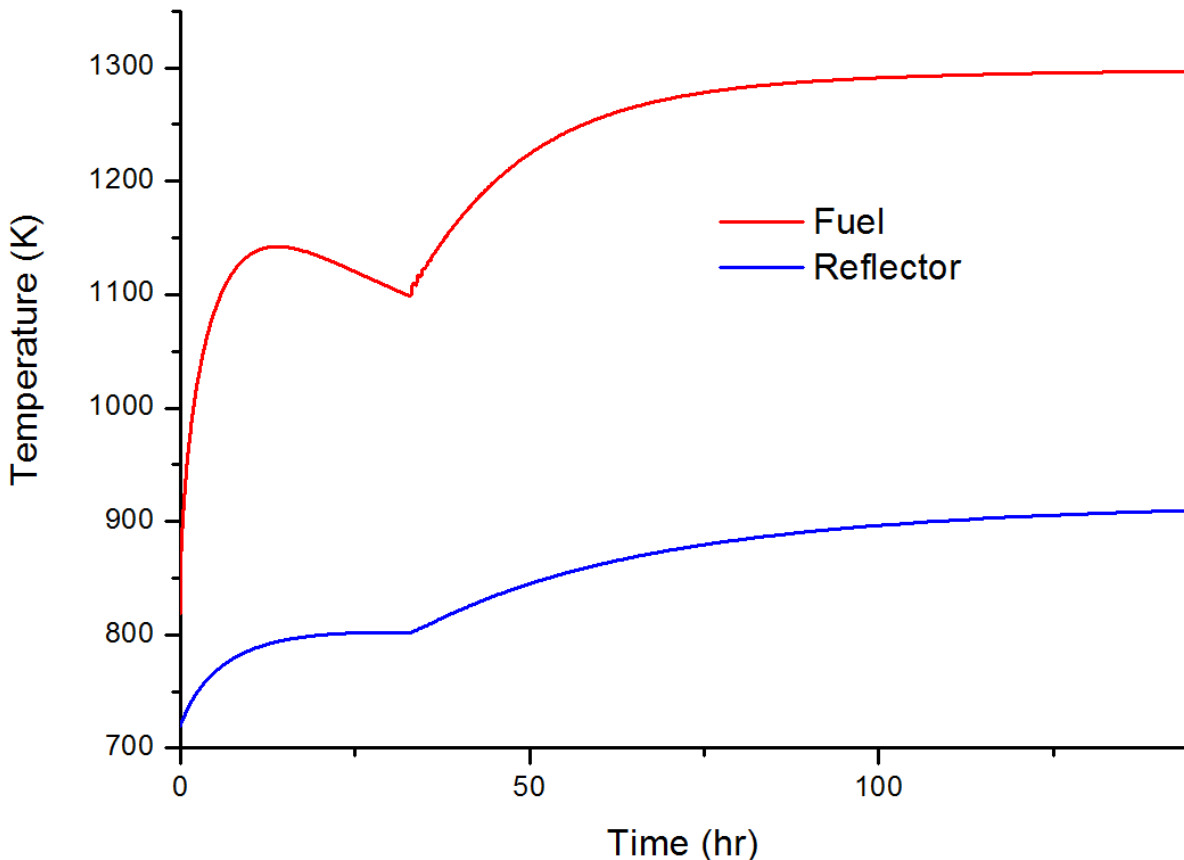


Figure 14. LOCA without scram transient

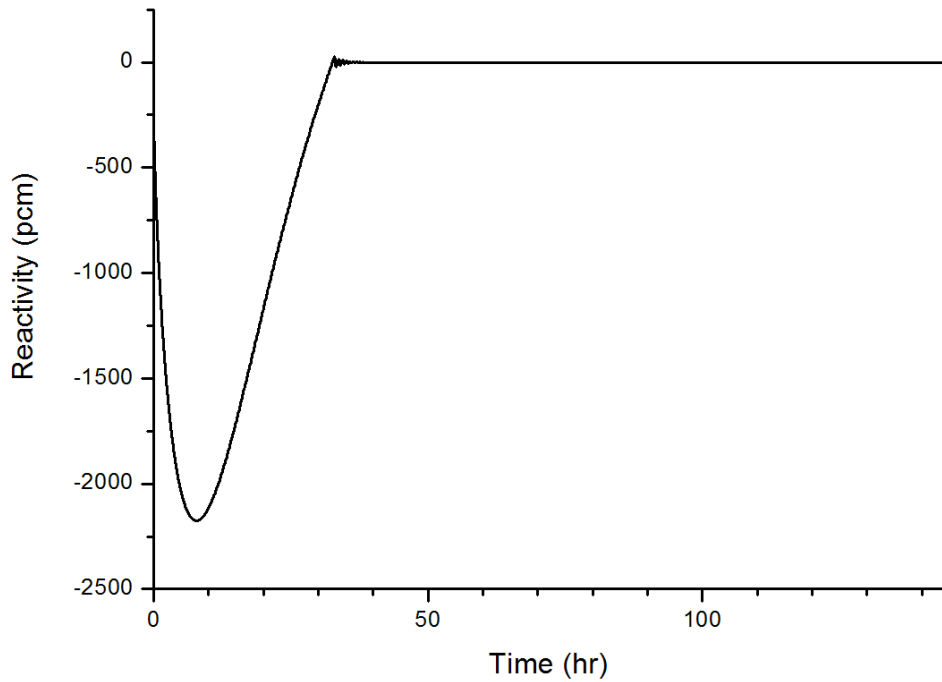


Figure 15. Core reactivity transient

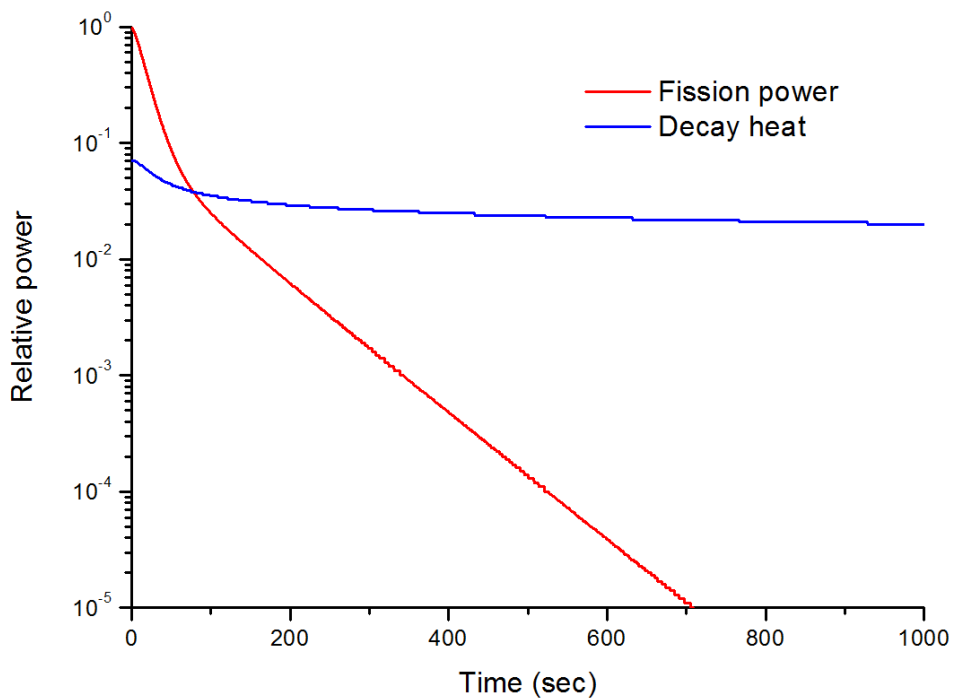


Figure 16. Fuel region power generation during LOCA

Figure 16 displays contributions of fission power and decay heat. The fission power decreases by point kinetics equation in long term. Initially, decay heat is about 7.1% of initial fission power. However, it drops very slowly that the decay heat contribution is significant after 80 seconds. This heat contributes to long term fuel temperature rise.

Reactor scram mechanism is required to prevent the fuel temperature rise to the equilibrium state at 1299K. Reactor scram before 30 hours will limit peak fuel temperature below 1142K.

Control rod ejection without trip

Control rod ejection without trip is an extreme event in a light water reactor. In a gas cooled reactor the micro kernel temperature rise is prompt so that the reactor will go subcritical much earlier than the larger pellet type fueled reactor. We analyzed the consequences of the control rod ejection accident by inserting 1000 pcm of external reactivity suddenly. Figure 17 - 19 displays the power transient, the temperatures, and the reactivity transient in short time. After control rod ejection, the reactor power rises promptly up to 30 times of the full power within 0.8 second as shown in Figure 17. This power rise induces fast temperature rise in kernel region as shown in Figure 18. The temperature rise in the kernel region is about 79K higher than that of the compact region. Fast kernel temperature rise introduces the negative Doppler feedback in short time as shown in Figure 19. The Doppler effect is effectively trip the reactor at 3.9 seconds without actual control rod trip.

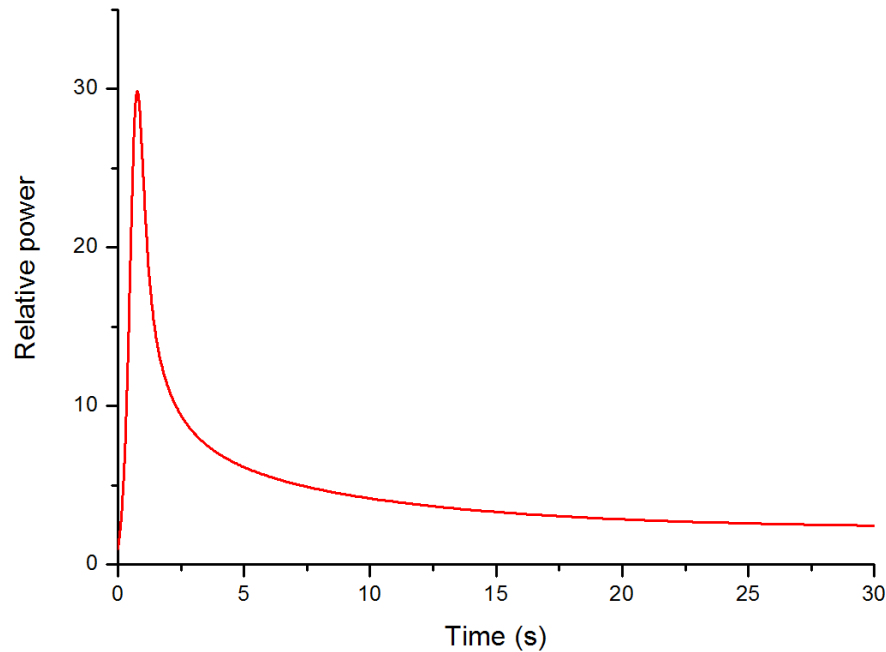


Figure 17. Power transient on control rod ejection

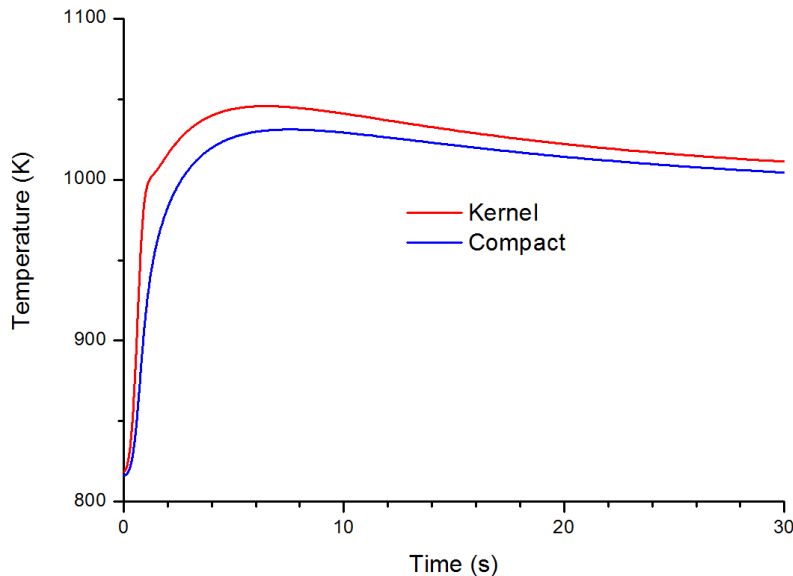


Figure 18. Temperature transient on control rod ejection

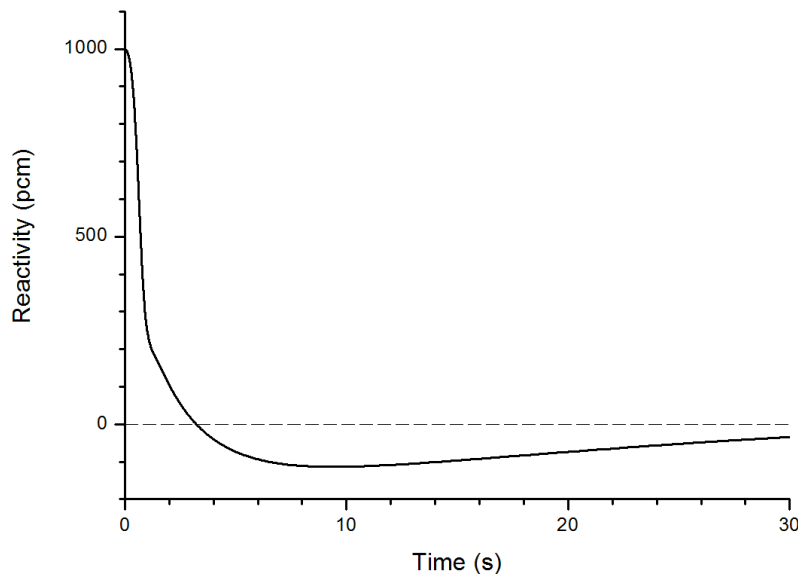


Figure 19. Short term reactivity transient on control rod ejection

In long term, kernel temperature drops by conducting heat to outside of TRISO. This effect makes the core criticality again. Figures 20-22 display the reactivity, power, xenon, and temperatures during few days without scram. The xenon built up during the short term excursion decays initially as shown in Figure 20. This process is slow. Decay of xenon introduces positive reactivity balanced by the increasing temperature. Reactor has sufficient time to produce thermal equilibrium power. When reactor power increases more xenon is produced so that negative

reactivity is inserted. This effect persists until about 13 hours. Strong xenon build up keeps the reactor in subcritical state. After 33 hours when xenon decays, the reactor becomes critical again.

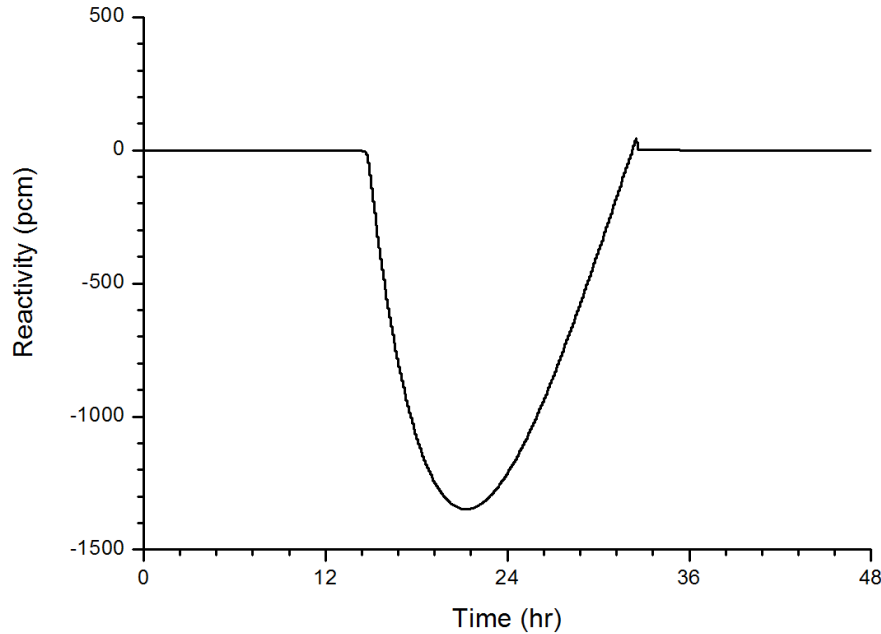


Figure 20. Reactivity transient on control rod ejection

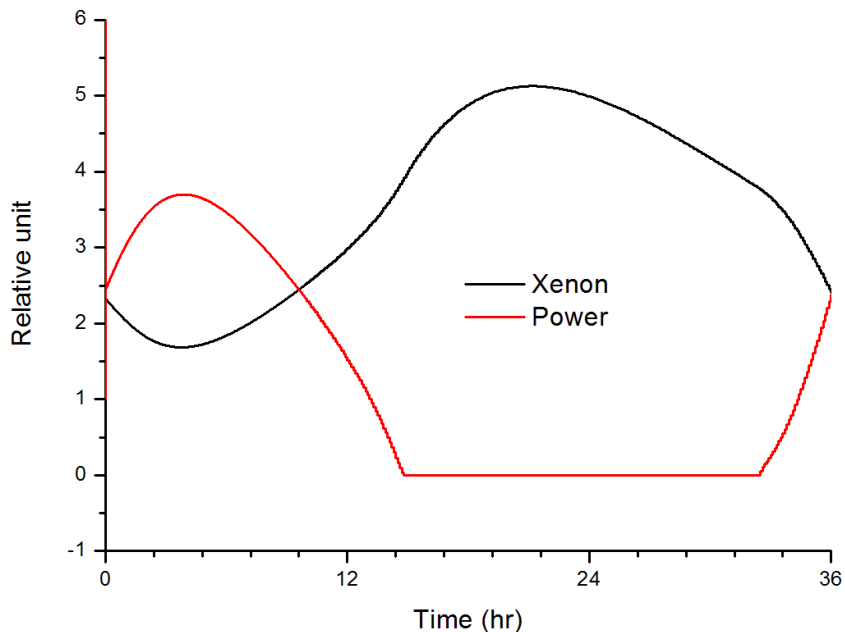


Figure 21. Power and Xenon transient on rod ejection

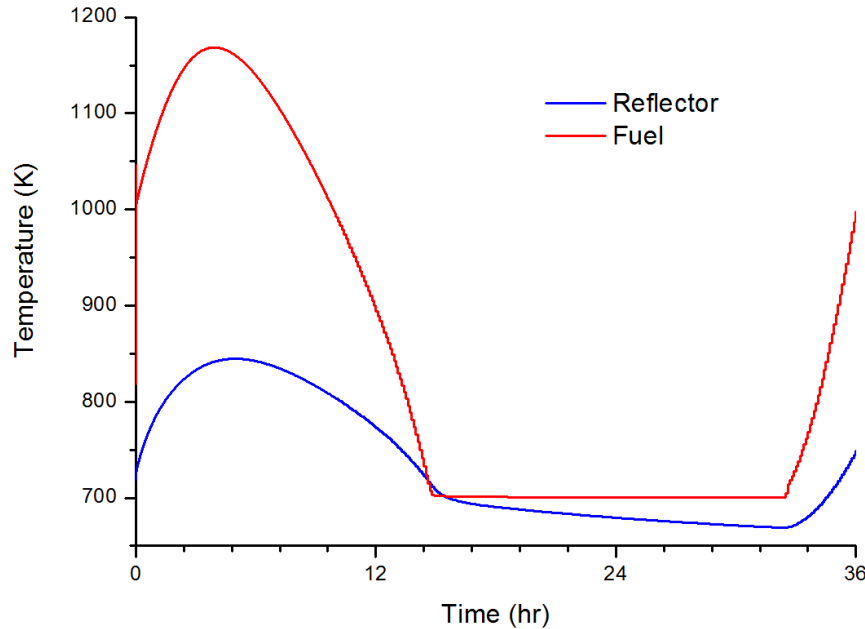


Figure 22. Temperature transient on rod ejection

Figure 23 displays long term behavior of reactor core during 4 days. It shows periodic behavior due to xenon oscillation coupled with core temperature redistribution. Peak power during oscillation does not exceed 3.1. Maximum fuel temperature does not exceed 1230K during oscillation. Fuel is intact during long term oscillation. Fission product release rate is exponentially proportional to fuel temperature. Proper scram before re-criticality, within a day, will prevent the second fuel temperature rise and limit radioactivity release to environment.

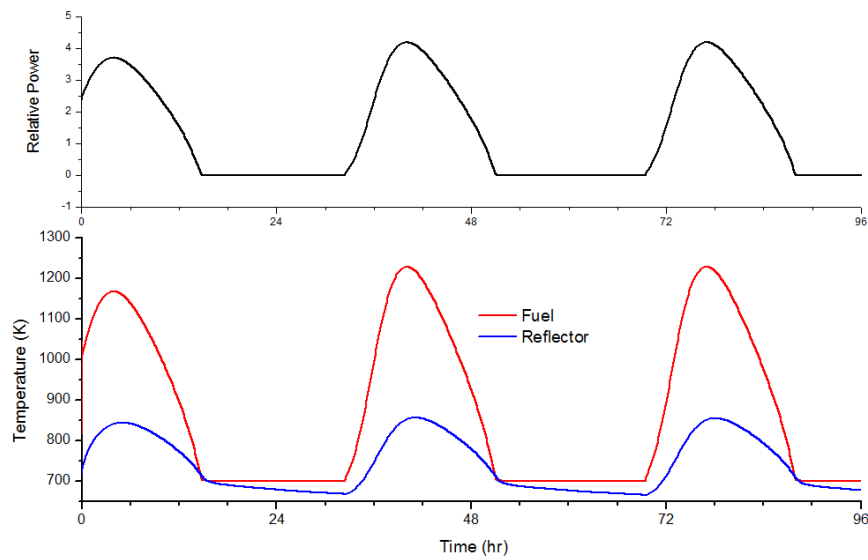


Figure 23. Long term transient of rod ejection accident

Summary

Current design of 40 MWth MMR with active core region of 2 m diameter and 2m height is limiting the average maximum fuel temperature below 1300K. Considering that TRISO is safe until 2000K, and conventional design limit of TRISO is 1620K(1350C), Current MMR-40 thermal design is acceptable. Abrupt disturbance in core will lead the reactor to sub-critical state and to reasonable peak fuel temperature. In long term, the reactor becomes re-critical to achieve next fuel temperature peak in few hours. Although the fuel is intact in long term, radioactivity release increases exponentially with fuel temperature. Un-necessary fuel temperature peak may be avoided by scrambling the reactor. The scrambling needs not be fast due to the negative Doppler feedback and the high heat capacity. Realistic feedback parameters derived from reactor physics analysis are needed to have more confidence on the result of thermal analysis.

References

- [Allaire, 2013] G. Allaire and Z. Habibi, Homogenization of a Conductive, Convective and Radiative Heat Transfer Problem in Heterogeneous Domain, SIAM J. of Math. Anal. 45(3), 1136-1178 (2013)
- [ANS-1994] American National Standard for Decay Heat Power in Light Water Reactors, ANSI/ANS-5.1-1994, ANS (1994)
- [Bank, 1985] R.E. Bank et al., Transient Simulation of Silicon Devices and Circuits, IEEE ED-32 (10) (1985)
- [Bensoussan, 1978] A. Bensoussan, J-L Lions, G. Papanicolaou, Aysmptotic Analysis for Periodic Structures, Chap1. 1978. in Studies in Mathematics and its Applications, vol.5, North-Holland.
- [Boer, 2009] B. Boer, Optimized Core Design and Fuel Management of a Pebble-Bed Type Nuclear Reactor, PhD thesis, TU Delft (2009)
- [CKjo, 2017] C. K. Jo, personal communication (2017)
- [Miller, 1993] G.K. Miller and R.G. Bennett, Analytical solution for stresses in TRISO-coated particles, J. Nucl. Mat. 206, 35-49 (1993)
- [Petti, 2004] D. Petti et al., Development of Improved Models and Design for Coated-Particle Gas Reactor Fuels: Final Report," INEEL/EXT-05-02615 (2004)
- [Stainsby, 2009] R. Stainsby, Investigation of Local Heat Transfer Phenomena in a Pebble Bed HTGR Core, NR001/RP/001 R01; Investigation of Local Heat Transfer Phenomena in a Prismatic Modular Reactor Core, NR001/RP/001 R02 (2009)
- [TECDOC-978] IAEA, Fuel performance and fission product behavior in gas reactors, IAEA-TECDOC-978 (1997)
- [TECDOC-1674] IAEA, Advances in High Temperature Gas Cooled Reactor Fuel Technology, IAEA-TECDOC-CD-1674 (2012)

4) Fuel performance analysis

Mechanical fuel performance analysis of a TRISO particle is important to estimate the fission product release fraction during normal operation and accident condition. We have developed a new performance analysis computer program for TRISO FCM fuel. Motivation of development are 1) to handle NITE SiC matrix which plays important role in FCM fuel, 2) to keep up-to-date with modern computer technology by rewriting computing model in C++ language rather than traditional Fortran language, 3) to make modular program which may be coupled in multi-physics frame easily. Results of the developed program was compared against IAEA benchmark problems.[TECDOC-1674]. The results of the IAEA benchmark problems were well reproduced.

Description of TRISO parameters

Table 5. MMR TRISO parameters

Layers	thickness(um)	density(g/cc)
UO ₂ Kernel diameter	800	10.8
Buffer	75	0.98
Inner PyC coating	35	1.85
SiC layer coating	36.7	3.2
Outer PyC coating	20	1.86
NITE SiC matrix	packing fraction 40%	

For MMR-40, the same TRISO parameters used in the safety analysis is used in this analysis as displayed in Table 1. Beside the geometric parameters, we need the irradiation time, the burnup, the neutron fluence, the FIMA (fissions per initial metal atom), and the nominal operation temperature. Those quantities and their maximum values are obtained from the reactor physics calculation. We did not perform the calculation yet. So we estimated maximum irradiation parameters evaluated from existing analysis for typical design such as PBMR, GTMHR, and NGNP. Adopted values are displayed on Table 6. Burnup and fluence is significantly smaller than conventional HTGR where reloading of fuel assembly is used for better utilization of nuclear fuel. However, in MMR concept, initial fuel is used until end of a cycle (in case of conventional HTGR) which is the core life time. Enrichment of MMR-40 fuel is 20%, so we assumed maximum FIMA as 20 %.

Table 6. Performance limit parameters for MMR-40

Quantity	Value	Unit
End of life (Effective full power days)	3670	days
EOL burnup	42.7	GWD/MTU
Fast fluence at EOL	1.3	10 ²⁵ n/m ²
Fission per initial metal atom (fima)	20	%
Mean operation temperature	1000	K

Development of fuel performance analysis code

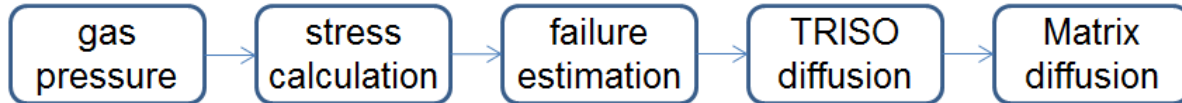


Figure 24. Fuel performance analysis model

Main objective of fuel performance analysis is to estimate the radioactivity release to environment or to the coolant. This analysis should be done starting from fission product source at kernel and others. Fission products are contained by coating layers such as IPyC, SiC, OPyC, and NITE-SiC matrix in a FCM fuel. When a coating layer is damaged, fission products will be released to next container. When the fission product is released to coolant, it can be easily released to environment through many leak paths. We have developed computer programs which can estimate the source to reactor coolant system.

Internal gas pressure

Internal gas pressure plays significant role in mechanical stress analysis of a TRISO particle. Gaseous molecules are accumulated in porous buffer region of a TRISO particle. A fission produces two kinds of molecules from lattice, the oxygen liberated from UO₂ kernel (or nitrogen liberated from UN kernel) and the fission products.

CO production.

In UO₂ kernel, two oxygen atoms are liberated by fission. This oxygen can be coupled with fission product, or remain as atomic oxygen. Atomic oxygen will diffuse through kernel and leaked to buffer region than become carbon mono-oxide. Carbon mono-oxide is important source of pressure in the buffer region.

There are several oxygen release model such as Proksch model[Proksch, 1982] and Homan model [Homan, 1978] based on experimental results. Considering validity range, we adopted simple Homan model which is only dependent on irradiation temperature. Atomic oxygen release per fission is calculated by [INL-02615]

$$O/f = 1.64e^{-3311/T}$$

$$\text{and } O/f_{\max} = 0.61$$

In other kernel form, such as UN, UC, or UCO, CO production is negligible.

Fission gas

We consider only krypton and xenon as fission gas. These gaseous isotopes decay into metallic elements such as rubidium or cesium.

Fission product are balanced by decay, neutron absorption, and fission yield, as follows

$$\frac{dN}{dt} = -\lambda N - \sigma_a N \phi + \eta \Sigma_f \phi .$$

In an equilibrium state, we have

$$N = \frac{\eta \Sigma_f \phi}{\lambda + \sigma_a \phi} .$$

When neutron absorption is negligible, the balance equation can be rewritten as

$$\frac{dN}{dt} = -\lambda N + \eta \Sigma_f \phi .$$

The equilibrium is written as

$$N = \frac{\eta \Sigma_f \phi}{\lambda} (1 - e^{-\lambda t}) .$$

To estimate the fission gas pressure, we selected isotopes with $\eta / \lambda > 1$, and stable isotopes with small neutron absorption cross sections.

Selected stable isotopes are Kr-84, -85, -86, and Xe-131, -132, -134, -136.

Table 7 and 8 display the properties of krypton and xenon isotopes relevant to fission gas pressure calculation. Decay chains are classified as;

- Type 0: stable isotope
- Type 1: daughter nuclide is stable
- Type 2: isomeric transition followed by subsequent decay
- Type 3: isomeric transition to stable isotope

Table 7. Kr isotopes from fission

Isotope	Half life	Decay constants	Yields		type	Remark
			U-235	Pu-239		
Kr-83	stable	0	5.381e-3	2.950e-3	0	
Kr-84	stable	0	1.035e-2	4.809e-3	0	
Kr-85m	4.48 h	1.867E-05	1.262e-2	5.589e-3	<input type="checkbox"/>	<input type="checkbox"/> 0.786, IT 0.214
Kr-85	3934.4 d	8.856E-10	4.152e-5	6.674e-5	-	
Kr-86	stable	0	1.973e-2	7.603e-3	0	
Kr-87	76.3 min	6.576E-05	2.515e-2	9.839e-3	1	
Kr-88	2.84h	2.944E-05	3.568e-2	1.325e-2	1	
Kr-89	3.15m	1.593E-03	4.611e-2	1.447e-2	1	
Kr-90	32.3s	9.320E-03	5.042e-2	4.635e-2	1	
Kr-91	8.57s	3.513E-02	3.396e-2	7.280e-3	1	

Table 8. Xe isotopes from fission

Isotope	Half life	Decay constant	Yields		type	Remark
			U-235	Pu-239		
Xe-131m	11.934d	2.920e-7	3.173e-4	4.236e-4	3	IT

xe-131	stable	0	2.884e-2	3.847e-2	-	
xe-132	stable	0	4.300e-2	5.393e-2	0	
xe-133m	2.19d	1.591e-6	1.949e-3	2.345e-3	2	IT
xe-133	5.243d	6.645e-7	6.702e-2	6.976e-2	-	
xe-134	stable	0	7.826e-2	7.631e-2	0	
Xe-135m	15.29m	3.281e-4	1.213e-2	1.883e-2	2	IT
Xe-135	9.14h	9.149e-6	5.318e-2	5.616e-2	-	
Xe-136	stable	0	6.306e-2	6.626e-2	0	
Xe-137	3.818m	1.314e-3	6.111e-2	6.073e-2	1	
xe-138	14.08m	3.563e-4	6.373e-2	5.081e-2	1	
Xe-139	39.68s	7.586e-3	5.141e-2	3.021e-2	1	

Significant nuclides which contribute to fission gas pressure are Kr-84, Kr-85, Kr-86, and xe-131, Xe-132, Xe-134, Xe-136.

Gas pressure model

Released fission gas and oxygen will migrate to buffer zone to build up a pressure in the porous carbon region. This migration can be calculated by diffusion model. For the purpose of mechanical stress analysis, we adopted simple assumption that the gas concentration is distributed homogeneously in the kernel and the buffer. This assumption is conservative one, since the concentration at the source region must be high and the leakage through IPyC is ignored.

The molar density is calculated as

$$\rho_m = \frac{N/N_A}{V_{ker} + V_{buf}}$$

where total numbers of gas molecules(atoms) N are calculated as sum of numbers obtained by CO production model and decay equation mentioned previously. V_{ker} and V_{buf} are volume of the kernel and the buffer zone, respectively.

We adopted Redlich-Kwong equation of states to calculate the fission gas pressure. Xe, Kr, and CO is considered.

$$P = \frac{RT}{V_m - b} - \frac{a}{\sqrt{T}V_m(V_m + b)}$$

Where P is the pressure(Pa). R is the gas constant. V_m is molar volume(m³/mol). T is the temperature (K).

Contants a, b are related to critical points of the gas as displayed at Table 9. [wiki: Redlich-Kwong equation of state]

Table 9. Redlich-Kwong EOS parameters

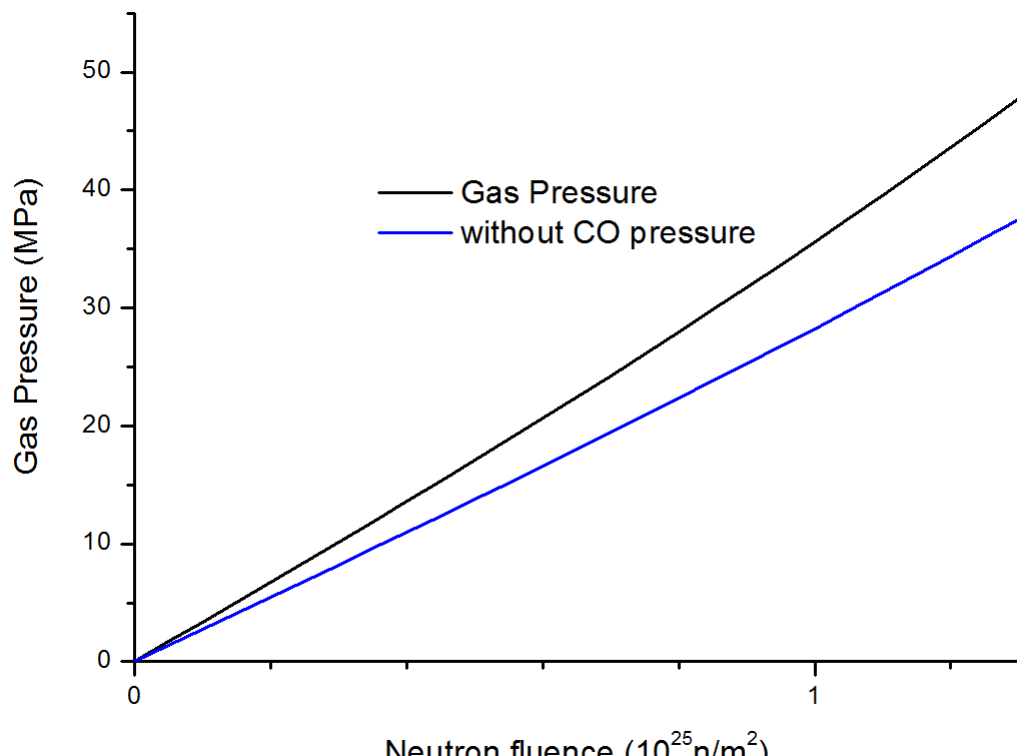
Gas	Tc (K)	Pc (MPa)	a	b
CO	132.91	3.5	1.72	2.736e-5
CO ₂	304.14	7.38	6.46	2.969e-5
Kr	209.45	5.5	3.411	2.743e-5
Xe	298.75	5.9	7.158	3.538e-5

For multiple components a and b is averaged by their molar fraction (x_i)

$$\bar{a}^{1/2} = \sum_{i=1}^n x_i a_i^{1/2}$$

$$\bar{b} = \sum_{i=1}^n x_i b_i$$

Results of the developed computer program were compared with the standard benchmark problems presented in TECDOC-1674. Figure 25 displays result of analysis. Buildup of gas pressure is almost linear as fluence (or time). UO₂ kernel has higher pressure than UN kernel due to CO gas buildup. Gas pressure of UN kernel is 21 % lower than UO₂ kernel.

**Figure 25. Fission gas pressure**

Stress analysis and failure estimation

For stress analysis, inner zone such as kernel and buffer are considered as an internal pressure boundary. The outer PyC coating is regarded as outer pressure boundary in usual stress analysis for TRISO fuel. However matrix material of a FCM fuel is dense NITE SiC which may contributes to stress distribution to inside coating layers. NITE SiC is modeled as an additional layer with equivalent thickness set by packing fraction. One dimensional spherical shell geometry is adopted in this study. SiC is regarded as an isotropic material but graphite is modeled as an anisotropic material. Graphite, and SiC, in some extent, develops creep at high temperature. Neutron irradiation at PyC graphite layers induces strain as well as creep. It is necessary to model this behavior reasonably accurate to understand mechanical behavior of coating layers. A kind of rheological model adopted for spherical TRISO coating is considering irradiation induced creep but neglecting transient creep.

For TRISO particle with spherical symmetry and non-isotropic material property, the equation of motion is written as following equations.

$$\frac{\partial \varepsilon_r}{\partial t} = \frac{1}{E} \left(\frac{\partial \sigma_r}{\partial t} - 2\mu \frac{\partial \sigma_t}{\partial t} \right) + c(\sigma_r - 2\nu\sigma_t) + \dot{S}_r ,$$

$$\frac{\partial \varepsilon_t}{\partial t} = \frac{1}{E} \left((1-\mu) \frac{\partial \sigma_t}{\partial t} - \mu \frac{\partial \sigma_r}{\partial t} \right) + c((1-\nu)\sigma_t - \nu\sigma_r) + \dot{S}_r ,$$

where,

t : fluence, not conventional time,

E : Young's modulus of elasticity,

μ : Poisson ratio,

c : steady-state creep coefficient,

ν : Poisson ratio in creep,

\dot{S} : strain induced by other reason such as irradiation induced dimensional change (IIDC) and thermal expansion term.

Strain-displacement relations is written as

$$\varepsilon_r = \frac{\partial u}{\partial r} ,$$

$$\varepsilon_t = \frac{u}{r} .$$

Stress equilibrium equation is written as

$$\frac{\partial \sigma_r}{\partial r} + \frac{2}{r}(\sigma_r - \sigma_t) = 0 .$$

This system of equations can be solved analytically. Steady irradiation creep problem is treated semi-analytically using Miller's approach. [Miller, 1993] Boer has derived a expression for the displacement in a spherical shell as follows. [Boer, 2009]

$$u(r,t) = K_0(r)p(t) + K_1(r)q(t) + K_2(r) \int p(t)cdt + K_3(r) \int q(t)cdt + K_4(r) \int \dot{S}_r(t)dt + K_5(r) \int \dot{S}_t(t)dt + K_6(r)F(t)$$

The function F is defined as serial sum of f_i as

$$F(t) = \sum_i f_i t^i$$

$p(t)$ and $q(t)$ are the radial stress at the inner surface and outer surface. At innermost shell, p is the internal pressure. At outermost shell q is the external pressure. The function $F(t)$ is zero at boundaries of shell.

Above relation can be reduced in simple form at inner and outer surface of a shell. The coefficients, which are found at Appendix C of Boer's thesis, are dependent on the shell radius and the mechanical property of the shell.

$$K_0(r) = -\frac{2r^3 r_a^3 (1-2\mu) + r_a^3 r_b^3 (1+\mu)}{2Er^2 (r_b^3 - r_a^3)}$$

$$K_1(r) = \frac{2r^3 r_b^3 (1-2\mu) + r_a^3 r_b^3 (1+\mu)}{2Er^2 (r_b^3 - r_a^3)}$$

$$K_2(r) = -\frac{2r^3 r_a^3 (1-2\nu) + r_a^3 r_b^3 (1+\nu)}{2r^2 (r_b^3 - r_a^3)}$$

$$K_3(r) = \frac{2r^3 r_b^3 (1-2\nu) + r_a^3 r_b^3 (1+\nu)}{2r^2 (r_b^3 - r_a^3)}$$

$$K_4(r) = \frac{r_a^3 r_b^3 \ln \frac{r_a}{r_b}}{r^2 (r_b^3 - r_a^3)} + \frac{r}{3}$$

$$K_5(r) = -\frac{r_a^3 r_b^3 \ln \frac{r_a}{r_b}}{r^2 (r_b^3 - r_a^3)} + \frac{2r}{3}$$

$$K_6(r) = \frac{2(\nu - \mu)}{3E(\nu - 1)} \left[\frac{r_b^3 (r^3 - r_a^3) \ln r_b - r_a^3 (r^3 - r_b^3) \ln r_a}{r^2 (r_b^3 - r_a^3)} - r \ln r \right]$$

Note that values of K_6 at both boundaries are zero.

We can solve a set of equations using continuity of the displacement and the radial stress between shell interfaces. IAEA recommended material property data are used in this study. Developed computer program was verified on IAEA numerical benchmark problems.[TECDOC-1674]

MMR-40 analysis

Material parameters are adopted from IAEA benchmark report[TECDOC-1674]. Material properties are assumed to be independent of the operation temperature and irradiation in this study. Table 10 displays the value used in this study.

Table 10. Material property for mechanical analysis

Material	PyC	SiC
Young's modulus (MPa)	3.96x10 ⁴	3.7 x10 ⁵
Poisson ratio(μ)	0.33	0.13
Creep coefficient (MPa/10 ²⁵ n/m ²)	4.93x10 ⁻⁴	-
Poisson ratio in creep(ν)	0.4	-
Thermal expansion (K ⁻¹)	5.50x10 ⁻⁶	4.90x10 ⁻⁶
Tensile strength (MPa)	200	873
Weibull modulus	5	8.02

Irradiation swelling strain rate of PyC is modeled as following polynomials. For fluence, x, less than 6.08x10²⁴ (n/m², E > 0.18 MeV),

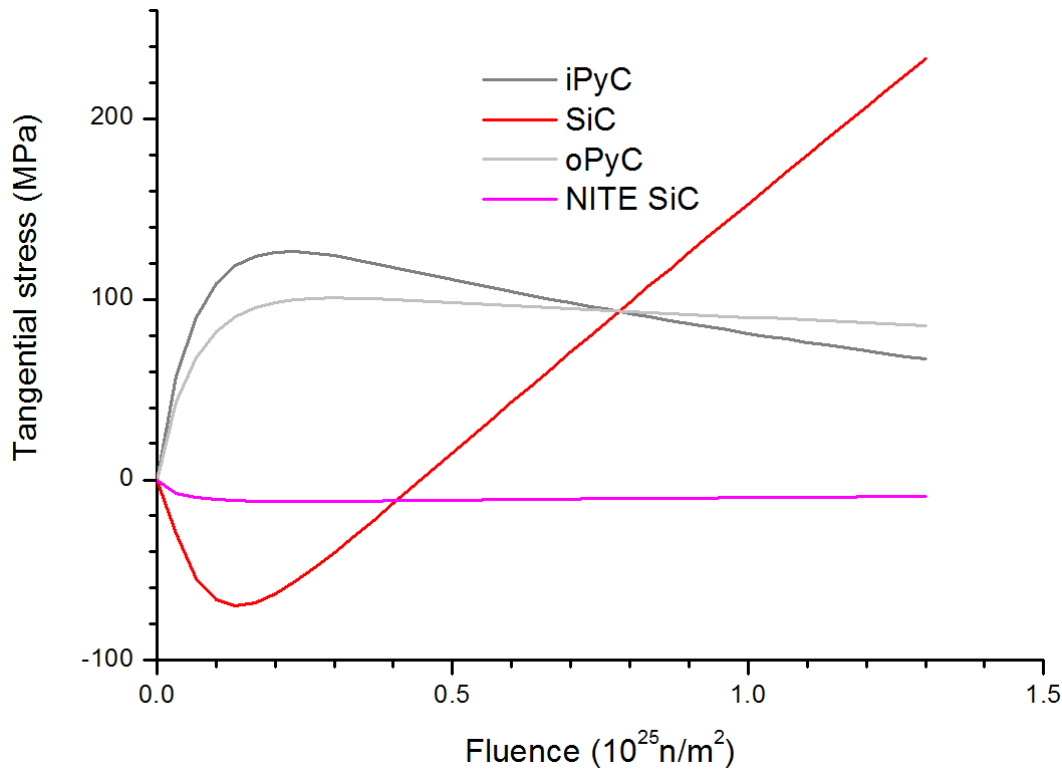
$$g_r = -1.43234 \times 10^{-1} + 2.62692 \times 10^{-1}x - 1.74247 \times 10^{-1}x^2 + 5.67549 \times 10^{-2}x^3 - 8.36313 \times 10^{-3}x^4 + 4.52013 \times 10^{-4}x^5$$

$$g_t = -3.23737 \times 10^{-2} + 9.07826 \times 10^{-3}x - 2.10029 \times 10^{-3}x^2 + 1.30457 \times 10^{-4}x^3$$

Material property of the NITE-SiC may be different from the pyrolytic SiC. However, NITE-SiC is dense composite of nano SiC crystals. Material property of NITTE SiC is not well known yet. We used the property of SiC coating layer as NITE SiC matrix in this study.

Slope of internal pressure increase is obtained from previous calculation on gas pressure. We adopt 36 MPa/(10²⁵ n/m²)

Figure 26 displays the variation of tangential stress along fluence. The tangential stress at inner surface of PyC coating is increasing sharply in early life. The peak is 126.4MPa at 0.23x10²⁵ n/m². Tangential stress on SiC coating layer is peaking -70 MPa and increases almost linearly. Tangential stress at the end of life is 233 MPa. This sharp increase is due to sharp increase in the internal gas pressure. The tangential stress on NITE SiC is less than 12 MPa.

**Figure 26. Tangential stress****Coating layer damage probability**

Weibull strength model is used to estimate the failure probability of each coating layer. The failure model is written as

$$\Phi = 1 - \exp \left[-\ln 2 \left(\frac{\sigma_t}{\sigma_0} \right)^m \right]$$

where, σ_t is the stress induced in the SiC layer, σ_0 is the tensile strength, m is the Weibull modules.

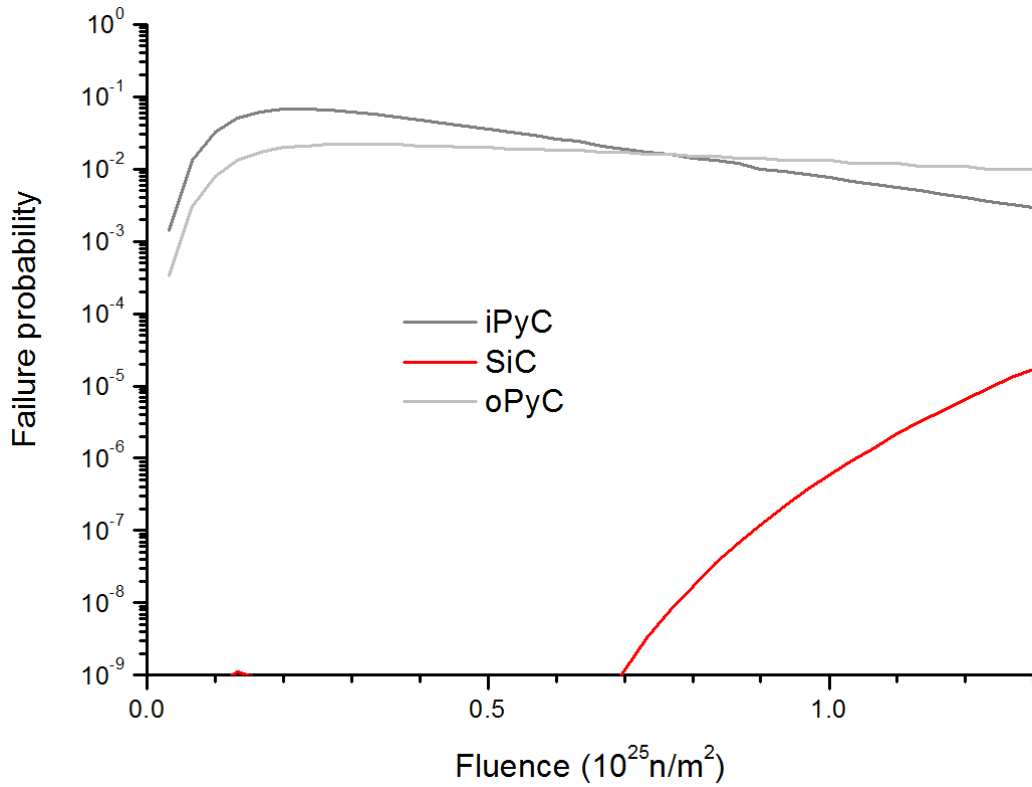


Figure 27. Failure probability of MMR TRISO

Figure 27 displays the failure probability of TRISO particle embedded in NITE SiC compact. Failure probability of iPyC coating rises sharply to 6.7%. Then the probability drops below the peak value. The failure on PyC coating is acceptable. The failure will mitigate stress on the SiC layer. However we neglect this effect for conservatism. SiC is regarded as actual fission product barrier. In most design the failure probability of SiC coating should be less 10^{-7} . Tentative design of TRISO for MMR violate this criterion. The failure probability of SiC coating layer increase to 1.7×10^{-5} . Sensitivity calculation shows that if we reduce the gas pressure to 2/3 of current level, the end of life failure probability drops to 1.3×10^{-7} . This target can be achieved either by increasing buffer thickness from 70 μm to 130 μm , or decrease enrichment from 20% to 14%.

Fission product transport analysis

Fission products produced in kernel region migrate through kernel, coating layers, etc., and decays as time goes by. The transport is a complex phenomenon which consists of the diffusion through tight crystal lattice, the leakage through cracks between tight crystals. These complex phenomena can be effectively treated with effective diffusion coefficient.

Fission product diffusion

Fission product diffusion is modeled as diffusion and decaying process. We adopted Stansby's approach to deal with heterogeneous diffusion problem.[Stansby, 2009] TRISO diffusion problem

is solved with reflective boundary condition with zero net production. Then matrix diffusion problem in cylindrical geometry handles the actual distribution and leakage of fission product. In matrix problem, metallic nuclides can be treated using diffusion trapping model. The diffusion – trapping – decay equation solved is written as follows.

$$\frac{\partial c}{\partial t} = D\nabla^2 c - \mu c + bm - \lambda c + s ,$$

$$\frac{\partial m}{\partial t} = \mu c - bm - \lambda m ,$$

where, c is concentration at diffusion site, m is concentration at trapping site, D is diffusion coefficient, μ is trapping coefficient, b is emission coefficient, and λ is decay constant, and s is the source. We cannot find suitable trapping model for NITE SiC matrix yet. So, we used diffusion only model in this study.

Table 13. Recommended IAEA diffusion coefficients.

	$D_{0,i}$ (m^2/s) $Q_{0,i}$ (kJ/mol)	Kernel	Buffer	PyC	SiC	Matrix graphite	Structural graphite
Ag	$D_{0,1}$	6.7×10^{-9}	10^{-8}	5.3×10^{-9}	3.6×10^{-9}	1.6	1.6
	$Q_{0,1}$	165	0	154	215	258	258
	$D_{0,2}$	-	-	-	-	-	-
	$Q_{0,2}$						
Cs	$D_{0,1}$	5.6×10^{-8}	10^{-8}	6.3×10^{-8}	$5.5 \times 10^{-14} \times e^{\Gamma/4.5}$ (b)	3.6×10^{-4}	1.7×10^{-6}
	$Q_{0,1}$	209	0	222	125	189	149
	$D_{0,2}$	5.2×10^{-4}	-	-	1.6×10^{-2}	-	-
	$Q_{0,2}$	362			514		
Kr	$D_{0,1}$	$1.3 \times 10^{-12} / 8.8 \times 10^{-15}$ (a)	10^{-8}	2.9×10^{-8}	$37 / 8.6 \times 10^{-10}$ (c)	6.0×10^6	6.0×10^6
	$Q_{0,1}$	126 / 54 (a)	0	291	657 / 326 (c)	0	0
	$D_{0,2}$	$0 / 6.0 \times 10^{-1}$ (a)	-	2.0×10^5	-	-	-
	$Q_{0,2}$	$0 / 480$ (a)		923			
Sr	$D_{0,1}$	2.2×10^{-3}	10^{-8}	2.3×10^{-6}	1.2×10^{-9}	10^{-2}	1.7×10^{-2}
	$Q_{0,1}$	488	0	197	205	303	268
	$D_{0,2}$	-	-	-	1.8×10^6	-	-
	$Q_{0,2}$				791		

a. First values used in irradiation conditions / Second values used in accidental conditions.

b. Γ : fast neutron fluence (10^{25} n/m^2 , $E > 0.18 \text{ MeV}$).

c. First values used above 1626 K / Second values used below 1626 K.

Figure 28. IAEA recommended diffusion coefficient[INL-EXT-14-33117]

The diffusion coefficient is generally modeled as follows.

$$D = \sum_i D_{0,i} \exp\left[-\frac{Q_i}{RT}\right] , \text{ where}$$

$D_{0,i}$ is the pre-exponential factor, Q_i is the activation energy, R is the gas constant, and T is the temperature.

We adopt the IAEA recommended effective diffusion coefficient values as given in Figure 28.

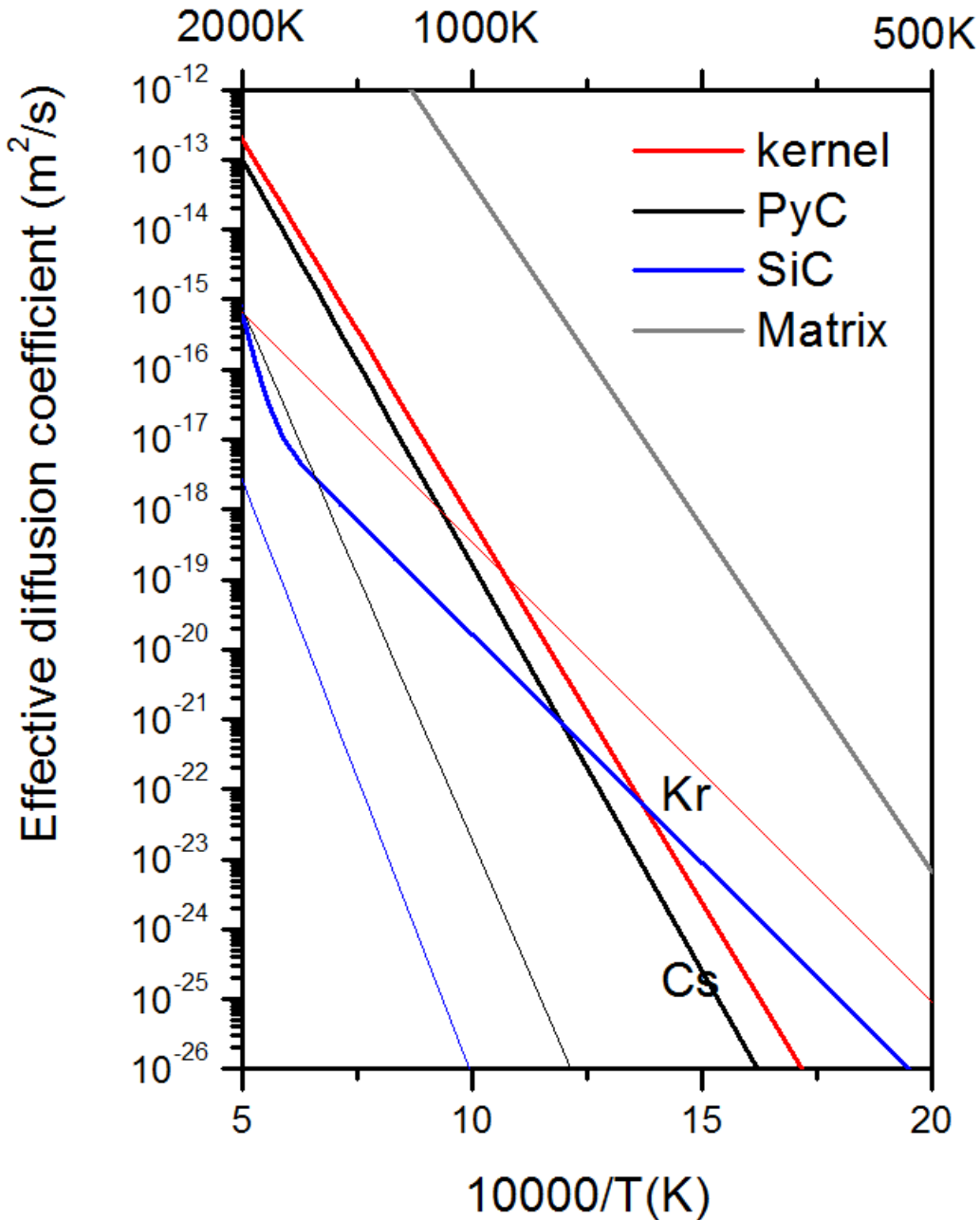


Figure 29. Effective diffusion coefficient (Thick line: Cs, Thin line: Kr)

Figure 29 shows the effective diffusion coefficients of cesium and krypton. In general, the diffusion coefficient in the graphite matrix is highest, that of kernel is the next, then that of PyC, and that of SiC is the lowest. Diffusion coefficient of cesium is higher than krypton in general.

Decay term is ignored in this study because the fission product concentration will be provided during depletion analysis when core design matures.

$$\frac{\partial c}{\partial t} = D \nabla^2 c + s$$

Above equation is a parabolic equation. Boundary condition of the equation is zero concentration at the outer boundary. Initial condition is given as concentration distribution. For normal operation, it is zero concentration. For accident analyses, the flat concentration distribution in the kernel and the buffer zone. Flat distribution will give higher leak rate than that of quasi-equilibrium distribution. TRBDF-2 is used to solve time dependent equation and a finite element method with quadratic base is used to solve the spatial dependency. There are several orders of difference in material zone. It is needed to subdivide nodes. Large differences in the diffusion coefficient introduce numerical instability. This instability is mitigated by decreasing the time steps.

The release to born ratio can be calculated using Gauss theorem.

$$R/B = 1 - \frac{4\pi \int_0^R c(r,t) r^2 dr}{B}$$

where, the birth rate is given as

$$B = 4\pi \int_0^R s(t) r^2 dr dt, \text{ for normal operation, and}$$

$$B = 4\pi \int_0^R c(r,0) r^2 dr, \text{ for accident situation.}$$

Fission product release model of MMR-40

We adopted the German diffusion coefficient model[IAEA-TECDIC-978]. TRISO in FCM is modeled by one dimensional spherical model added by equivalent radius of matrix material. This assumption will give the average release fraction with reasonable accuracy.

We calculated R/B ratio of two representative atoms, cesium and krypton. Cesium is important due to long term radioactivity. The release of radioactive cesium impact significantly damage of environmental contamination. Krypton is a representative noble gas which is used to monitor the release during operation and accident.

Normal operation

During normal operation, TRISO temperature is almost kept constant. The temperature is set to 900K which is higher than average temperature of core but reasonably conservative to estimate release during normal operation. Fluence is increasing linearly along burnup. End of life (EOL) fluence is $1.3 \times 10^{21} n/cm^2$ at 3670 days as displayed at Table 2. Diffusion coefficient of SiC is varying due to depletion.

Figures 30 and 31 display the R/B (release to birth) ratio of cesium and krypton isotopes, respectively. Kernel holds fission products significantly. R/B ratios of intact FCM TRISO for Cs and Kr are 1.1×10^{-6} and 1.4×10^{-6} , respectively, at the end of life. On PyC coating layers failed, the

leak rates for Cs and Kr increase to 5×10^{-6} and 8×10^{-6} , respectively. Even though all coating layer fail, when NITE SiC is intact, the R/B ratio for Cs and Kr increase to 5.3×10^{-6} and 1.2×10^{-5} , respectively. For graphite matrix, the R/B ratio of completely damaged coating layer for Cs and Kr are 2×10^{-2} and 2.2×10^{-3} , respectively. Thus, NITE SiC matrix reduces the leak ratio to 100 times or more compare to conventional graphite matrix.

The reliability of the diffusion coefficient for NITE SiC is important for reliable estimation of R/B ratio. R/B ratio can be further reduced by increasing effective matrix thickness, in other word, reducing the packing fraction.

Accident situation

For accident condition, we assume average kernel temperature during normal operation. This assumption results more fission product remained in a FCM fuel, so that more fission product can be released during accident.

We simulated accident condition by taking temperature transient obtained from the safety analysis on LOCA which results in highest transient temperature (Fig. 32).

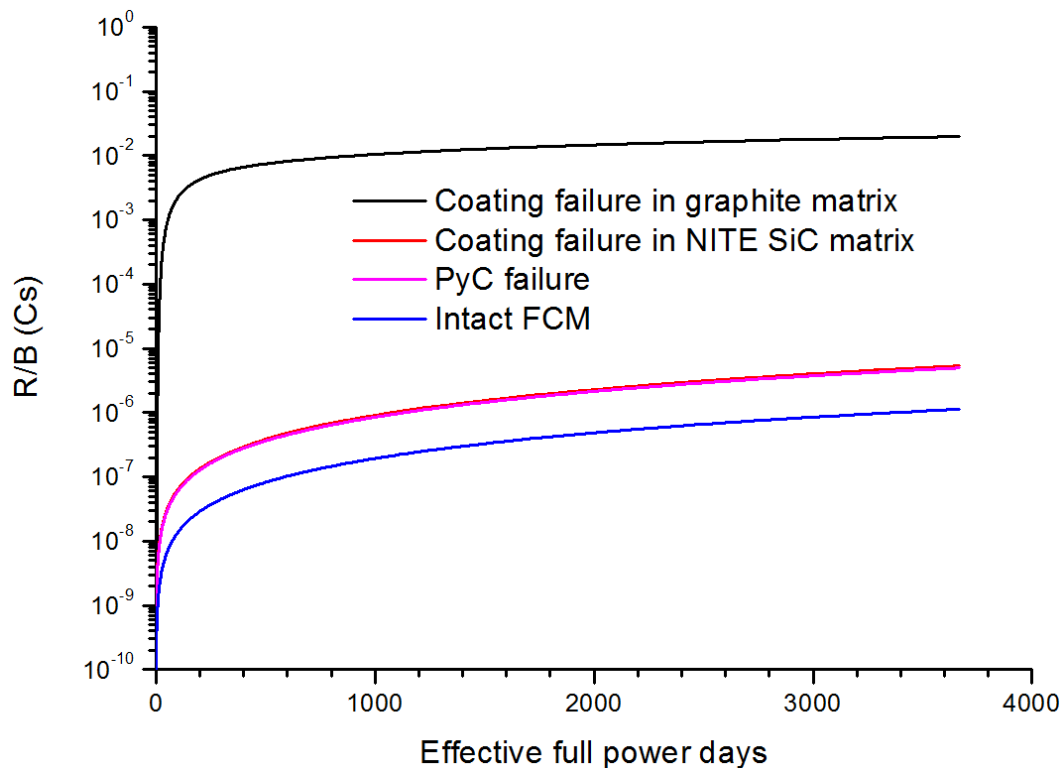
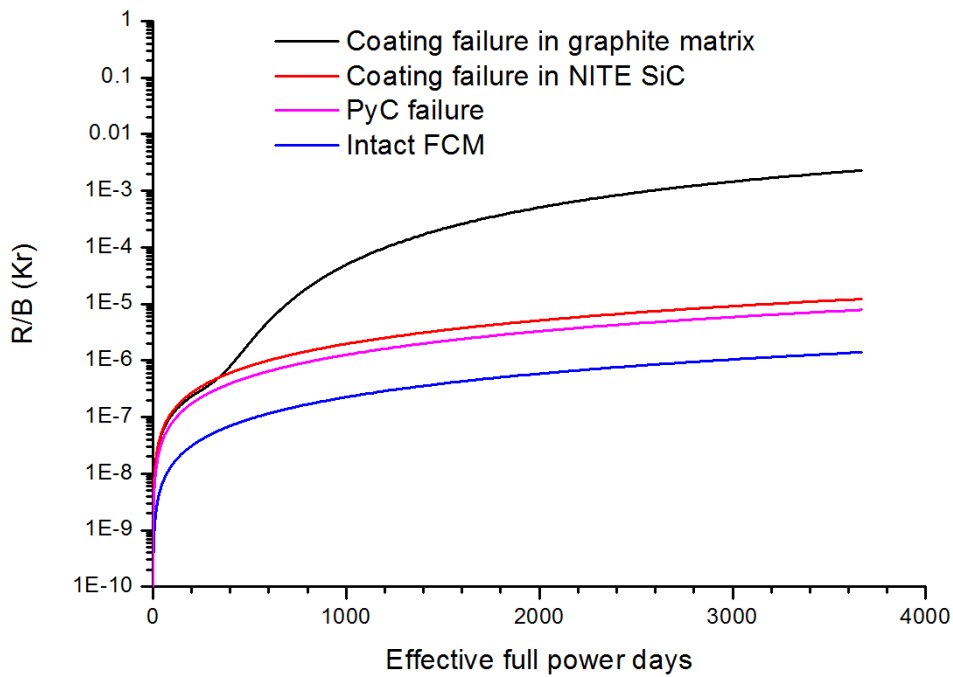
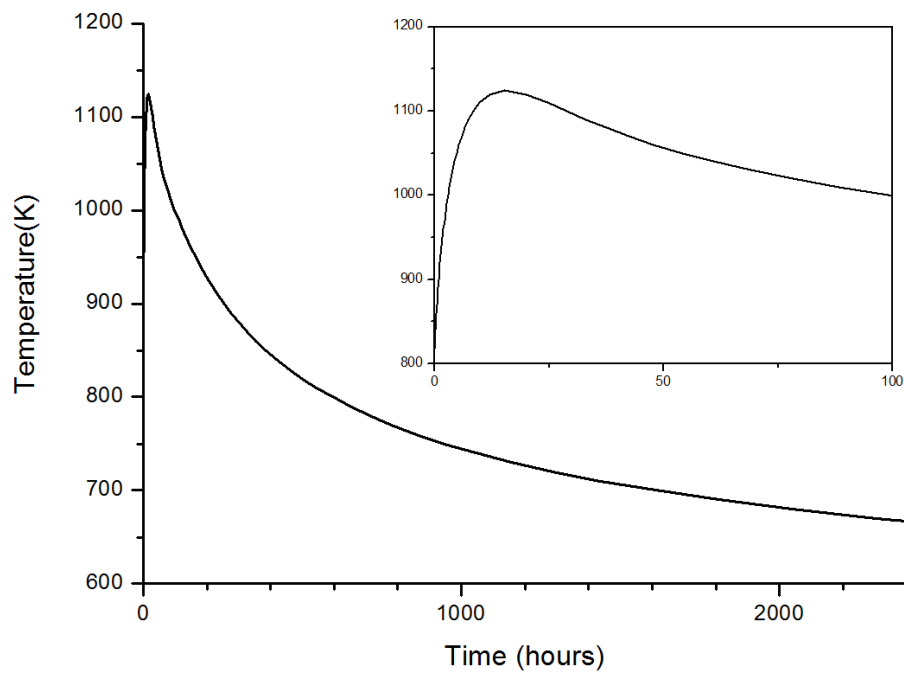


Figure 30. R/B of cesium

**Figure 31. R/B of krypton****Figure 32. Temperature variation during LOCA**

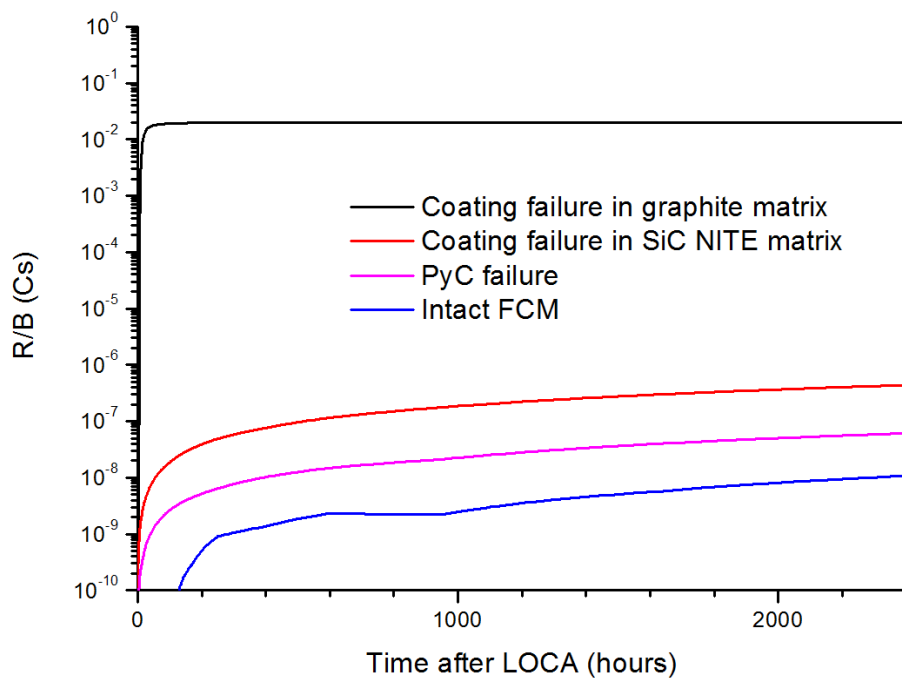


Figure 33. R/B of cesium during LOCA

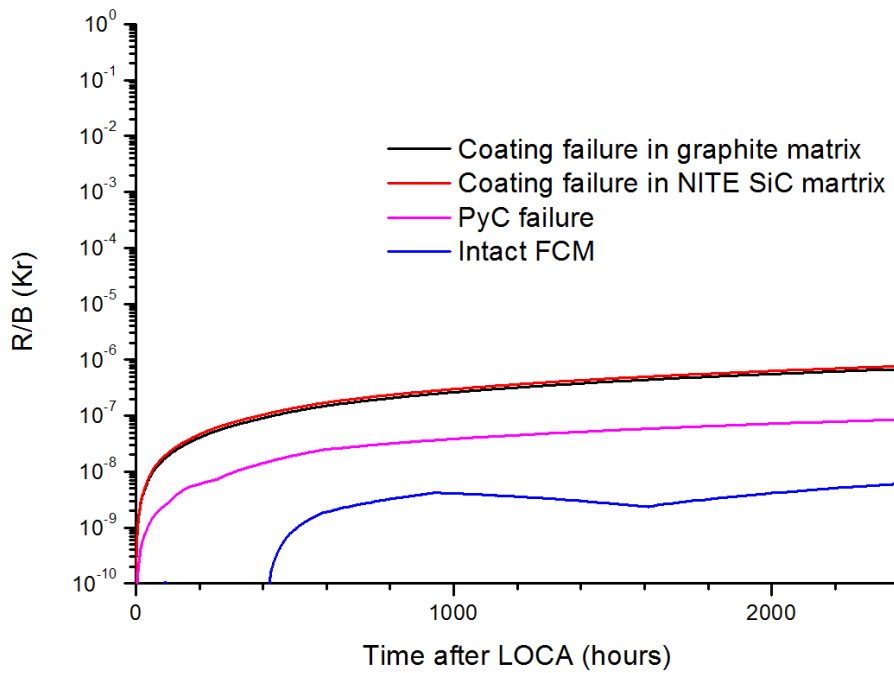


Figure 34. R/B of krypton during LOCA

Figures 33 and 34 display the R/B ratio of cesium and krypton. Each calculation is repeated for the intact TRISO, the damaged PyC coating layers, and the complete failure in coating layers for SiC NITE FCM. A calculation is performed for the complete failure in coating layers for the graphite matrix.

The increase of R/B ratio is about ten-fold when coating layer fails. R/B ratio of cesium reveals the advantage of NITE-SiC FCM fuel. However the discrepancy in R/B of krypton is not much. The R/B ratio of FCM fuel is below 10^{-6} even with complete loss of coating layers.

Summary of fuel performance analysis

Model analysis shows that the failure probability of SiC coating layer FCM increase to 1.7×10^{-5} . This figure is relatively large value comparing that of conventional TRISO is 10^{-6} or below. High failure rate is largely due to high pressure in the buffer region. It is recommended to increase buffer volume of TRISO for high enrichment, or to use uranium nitride kernel which do not produce liberated oxygen.

Even though all coating layer fail, when NITE SiC matrix is intact, the R/B ratio for Cs and Kr increase to 5.3×10^{-6} and 1.2×10^{-5} , respectively. During LOCA, R/B ratio of failed TRISO particle remains below 10^{-6} due to strong retention capability of NITE SiC FCM. However the supporting diffusion experiments for NITE-SiC are not available during this study. It is recommended to develop a reliable diffusion model for NITE-SiC based on experiment to be used in MMR FCM.

References

- [ANS-1994] American National Standard for Decay Heat Power in Light Water Reactors, ANSI/ANS-5.1-1994, ANS (1994)
- [Boer, 2009] B. Boer, Optimized Core Design and Fuel Management of a Pebble-Bed Type Nuclear Reactor, PhD thesis, TU Delft (2009)
- [Homan, 1978] F. Homan, H. Nabielek and L. Yang, "Low-enriched Fuel Particle Performance Review," GA-A14759 (1978)
- [INL-02615] D. Petti, et al., "Development Of Improved Models And Designs For Coated-Particle Gas Reactor Fuels: Final Report," INEEL/EXT-05-02615, INL, Dec. 2004.
- [Miller, 1993] G.K. Miller and R.G. Bennett, Analytical solution for stresses in TRISO-coated particles, J. Nucl. Mat. 206, 35-49 (1993)
- [Proksch, 1982] E. Proksch, A. Strigl, and H. Nabielek, "Production of Carbon Monoxide during Burn-up of UO₂ Kernelled HTR Fuel Particles," J. Nucl. Mat. 107, 280-285 (1982)
- [Stainsby, 2009] R. Stainsby, Investigation of Local Heat Transfer Phenomena in a Pebble Bed HTGR Core, NR001/RP/002 R01; Investigation of Local Heat Transfer Phenomena in a Prismatic Modular Reactor Core, NR001/RP/001 R02 (2009)
- [TECDOC-978] IAEA, Fuel performance and fission product behavior in gas reactors, IAEA-TECDOC-978 (1997)
- [TECDOC-1674] IAEA, Advances in High Temperature Gas Cooled Reactor Fuel Technology, IAEA-TECDOC-CD-1674 (2012)

5) Licensing approach

The licensing approach for the MDP-MMR is derived from its design approach to safety. A key design feature of the MDP-MMR that allows for high-temperature operation with inherent safety is the use of ceramic, coated particle fuel. A coated fuel particle consists of a microsphere (“kernel”) of nuclear fuel (usually in the form of an oxide, carbide, or oxycarbide) that is coated with multiple layers of pyrolytic carbon and silicon carbide. The buffer, inner pyrolytic carbon (IPyC), silicon carbide (SiC), and outer pyrolytic carbon (OPyC) layers are referred to collectively as a TRISO coating. The coating system can be viewed as a miniature pressure vessel that provides primary containment of radionuclides, even at the very high temperatures experienced during normal operation and postulated accidents with loss of cooling. As shown in Fig. 35, the TRISO-coated fuel particles are consolidated into fuel pellets. For the MDP-MMR, the fuel pellet is a SiC matrix that provides an additional defense-in-depth barrier to radionuclide release and chemical attack relative to a conventional pellet manufactured from carbonaceous materials. The fuel pellets, referred to as Fully Ceramic Microencapsulated (FCM) fuel, are loaded into graphite fuel blocks.

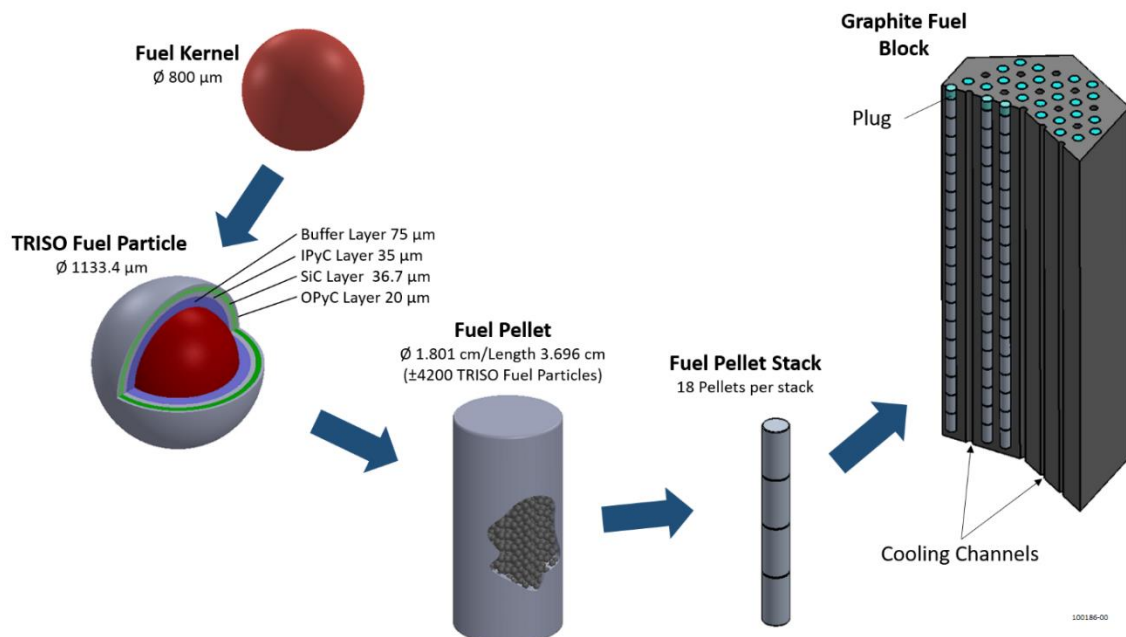


Figure 35. MDP-MMR Fuel Element Components

The MDP-MMR is designed with both passive and inherent safety features. Inherent safety features include:

- FCM fuel
- Graphite core with high heat capacity and large surface area for heat transfer
- Low power density
- Inert helium coolant, which reduces circulating and plateout activity
- Negative temperature coefficients of reactivity
- Multiple barriers to the release of radionuclides, starting with the FCM fuel

MDP-MMR heat removal systems provide active, passive, and inherent safety. The main heat transport system functions as an active system for decay heat removal. Passive and inherent safety heat removal are illustrated in Fig. 36. In the event the main heat transport system is unavailable, the passive Reactor Cavity Cooling System (RCCS) can remove decay heat using natural convection. In the event the RCCS is unavailable, direct heat transfer to the surrounding environment can maintain fuel temperatures well below damage limits to provide inherent safety.

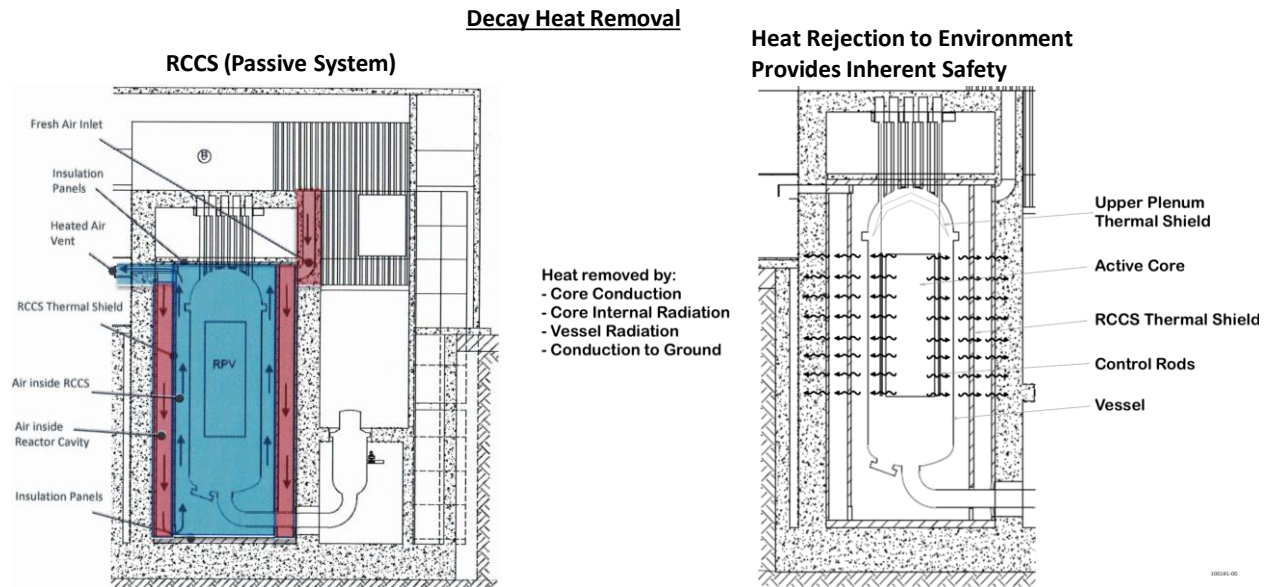


Figure 36. Passive and Inherent Safety Decay Heat Removal

Figure 37 shows the transient response of fuel temperatures during loss of flow (system pressurized) and loss of coolant accidents (system depressurized). The combination of a graphite reactor core with high heat capacity and low power density results in limited fuel temperature

transients that occur slowly over time periods of several days during loss of flow or loss of coolant accidents. This allows for measures to restore a more rapid cool down and return to normal operation.

A fundamental requirement for MDP-MMR safety design is to eliminate the need for public evacuation, regardless of the severity of any accident, without requiring any active measures. To satisfy this requirement, the regulatory requirements for allowable radiation dose to the public are applied at the plant boundary. This means a person standing next to the fence that defines the plant boundary could remain there throughout the course of a severe accident and will not receive a radiation dose that exceeded regulatory limits.

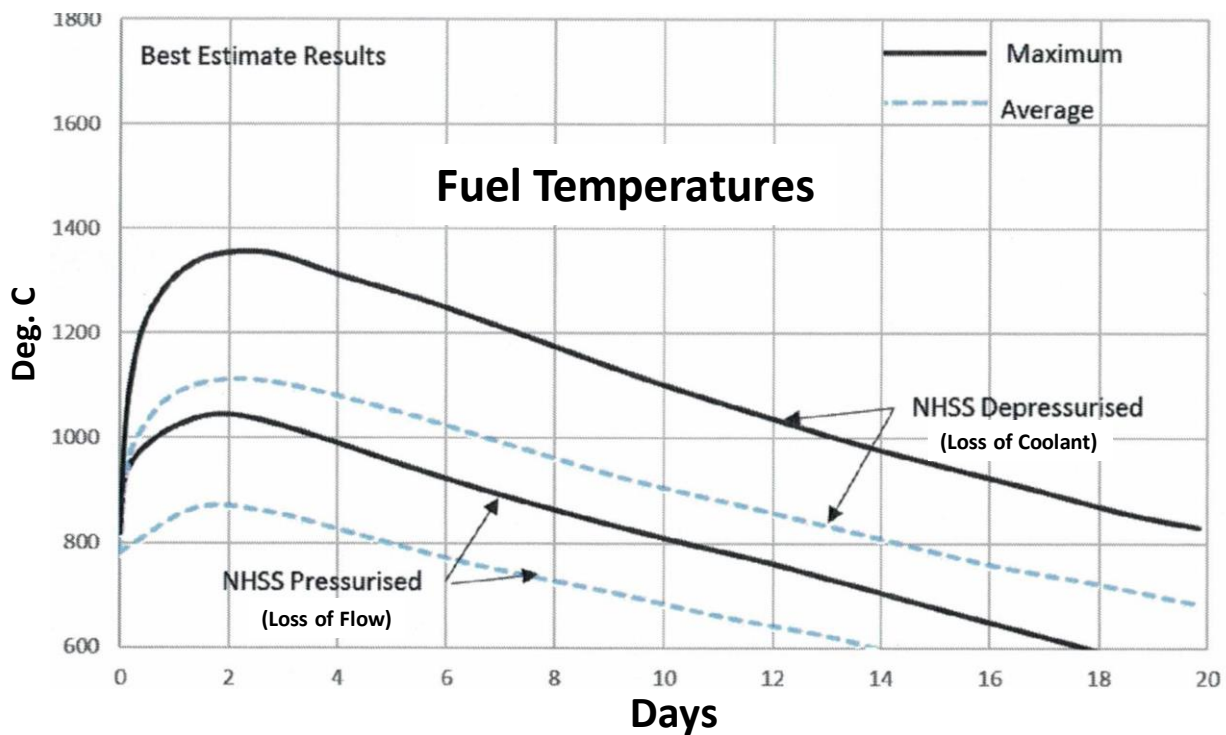


Figure 37. Fuel Temperature Response during Loss of Flow and Loss of Coolant Events.

A mechanistic approach is used to determine the radionuclide source terms for estimating radiation doses. A systematic process is used, starting with the imposed regulatory criteria for both off-site dose to the public and worker dose to ultimately define radionuclide design criteria, accounting for the multiple release barriers (functional containment approach), starting with the

FCM fuel. The off-site dose limits provide the most limiting constraints on these barriers. In the U.S., the requirements imposed by the Environmental Protection Agency Protective Action Guides (PAGs) for accidents are the most limiting requirements. The EPA imposes a limit of < 10 mSv (1 rem) Total Dose Effective Equivalent (TEDI) and < 50 mSv (5 rem) thyroid dose. For the MDP-MMR, these requirements are imposed at the plant boundary.

The FCM fuel provides the primary barrier, but there is a very small level of release to the primary coolant. Condensable radionuclides, including fission metals and iodine isotopes can plateout on the cooler surfaces of the primary circuit, and become a source term during depressurization events. The reactor building can provide a barrier through condensation, deposition, and settling.

Radioactivity released during an accident can be categorized into prompt and delayed source terms. The prompt source term is comprised of both circulating and plateout radioactivity. Circulating radioactivity is comprised of mostly noble gases that can be released during a primary coolant depressurization event. Plateout radioactivity is comprised of mostly condensable radionuclides (e.g., I-131) that plateout on the cooler wetted surfaces of the primary coolant circuit. Plateout activity can be released as the result of surface shear forces during a rapid depressurization event (large break of the primary coolant pressure boundary). The time scale for the prompt source term ranges from seconds to minutes.

The delayed source term results from the very slow heatup of the core during a severe accident, as illustrated in Fig. 32. The delayed source term develops over the course of the heatup portion of the transient and consists primarily of radioactivity released from heavy metal contamination, the very small fraction of defective fuel particles that may fail during normal operation, and the very small fraction of non-defective particles that may fail during normal operation and during the heatup. The time scale for the delayed source term ranges up to several days. Because of the nature of the delayed source term, the design of the reactor building is another inherent safety feature for further mitigating radioactivity release during a severe accident. For these types of accidents, the radiological consequences are reduced by allowing the reactor building to vent at a low differential pressure, resulting in a slow, low-concentration release from the reactor building.

NGNP Licensing Approach

The Next Generation Nuclear Plant (NGNP) project represents the most recent detailed interactions between the Department of Energy (DOE) and the Nuclear Regulatory Commission (NRC) to evaluate regulatory requirements for licensing a specific advanced (non-LWR) reactor

concept with enhanced safety characteristics relative to conventional power reactors deployed in the U.S. The NGNP conceptual design is a modular HTGR, with a module thermal power level of 350 MW, a primary coolant outlet temperature of 725°C, and primary coolant pressure of 7 MPa [NGNP 2011].

The NGNP project included a significant number of pre-application interactions with the NRC, including submittal of eleven licensing white papers on key topics of interest to the NRC. These papers are listed in Table 11. As indicated in Table 1, the NGNP project adopted a risk-informed, performance-based (RIPB) licensing approach. Key features of this approach are described below:

- Use of accident frequency vs. radiological dose criteria that are derived from current U.S. licensing requirements, referred to as Top Level Regulatory Criteria (TLRC).
- Use of a full-scope Probabilistic Risk Assessment (PRA) that is anchored to technically sound, deterministic engineering bases to select the Licensing Basis Events (LBEs).
- Development of reactor-specific functions, selection of the corresponding safety-related Structures, Systems, and Components (SSCs), and their regulatory design criteria.
- Deterministic Design Basis Accidents (DBAs) and special treatment requirements for the safety-related SSCs.
- Safety analyses based on mechanistic source terms and conservative assumptions to confirm that the TLRC dose limits are met with acceptable safety margins for DBAs.
- Risk-informed evaluation of defense-in-depth.

Table 11. NGNP Licensing White Papers

Title	Document No.	Submittal Date
RIPB Licensing Approach		
Licensing Basis Event Selection	INL/EXT-10-19521	Nov. 2, 2010
Structures, Systems, and Components Safety Classification	INL/EXT-10-19509	Nov. 2, 2010
Probabilistic Risk Assessment	INL/EXT-11-21270	Sept. 20, 2011
Defense in Depth	INL/EXT-09-17139	Dec. 9, 2009

Fuel Performance and Mechanistic Source Terms		
Fuel Qualification	INL/EXT-10-18610	July 21, 2010
Mechanistic Source Terms	INL/EXT-10-17997	July 21, 2010
Emergency Planning		
Determining the Appropriate EPZ Size and Emergency Planning Attributes for an HTGR	INL/MIS-10-19799	Jan. 26, 2011
Safety and Design – Other		
High Temperature Materials	INL/EXT-09-17187	June 25, 2010
Modular HTGR Safety Basis and Approach	INL/EXT-11-22708	Sept. 6, 2011
Licensing Structure		
Licensing Structure for Multi-Module Facilities	INL/EXT-10-18178	Aug. 10, 2010
Industrial Facility and Design Certification Boundaries	INL/EXT-11-21605	July 22, 2011

New nuclear power plants can be licensed under either of two existing regulatory approaches. The first approach is the traditional “two-step” process described in 10CFR50, “Domestic Licensing of Production and Utilization Facilities,” which requires both a construction permit and a separate operating license. The second approach is the “one-step” licensing process described in 10CFR52, “Licenses, Certifications, and Approvals for Nuclear Power Plants,” which incorporates a combined Construction and Operating License (COL). Both of these processes allow either a deterministic or a RIPB approach to satisfy technical requirements. The NGNP project adopted the 10CFR52 COL process, in part to reduce licensing schedule risk and financial risk to the owner/operator of the nuclear power plant. Successful licensing, construction, and operation of the initial demonstration plant will directly support future replication and deployment of multiple commercial plants. Lessons learned from licensing, construction, and testing of the demonstration plant are incorporated into the commercial plant design as part of its Design Certification (DC). The DC can then be referenced by future commercial plant COL applications. The NGNP licensing approach is described in more detail in the NGNP Licensing Plan [INL 2009] and in the NGNP Conceptual Design Report [NGNP 2011].

NRC Assessment of NGNP Key Licensing Issues

On July 17, 2014, the NRC issued a letter report to DOE [NRC 2014] on assessment by the NRC staff of key NGNP licensing issues, including specific assessments of the white paper submittals on fuel qualification and mechanistic source terms. Feedback from the NRC staff included the following:

- “In summary, the staff views the proposed high-level approaches to NGNP fuel qualification and mechanistic source terms as generally reasonable. The staff observes that the fuel development and testing activities completed to date in the AGR Fuel Program appear to have been conducted in a rigorous manner and with early results that show promise towards demonstrating much of the desired retention capability of the TRISO particle fuel developed for NGNP. Moreover, the staff believes that the planned scope of activities in the AGR Fuel Program is reasonably complete within the context of pre-prototype fuel testing.”
- “The NRC staff’s FQ-MST [Fuel Qualification-Mechanistic Source Term] assessment report concludes, with caveats, that DOE/INL’s ongoing and planned testing and research activities for NGNP fuel qualification and mechanistic source terms development appears to constitute a reasonable approach to establishing a technical basis for the identification and evaluation of key HTGR fission product transport phenomena and associated uncertainties. The staff expects more information on release and transport phenomena through event sequence-specific pathways to be developed as DOE/INL’s activities in these areas proceed.”

The “caveats” noted in the NRC assessment pertain primarily to the staff’s perceived need for fuel surveillance and testing of fuel fabricated in the production fuel facility and taken from the initial core of the prototype HTGR.

For the NGNP project, fuel qualification is being performed under the Advanced Gas Reactor (AGR) Fuel Development and Qualification Program [NL 2016]. The NRC feedback summarized above is based in part on a detailed review of this fuel qualification plan. The MDP-MMR fuel qualification plan will also require review by NRC staff as part of any U.S. licensing effort.

Recent DOE/NRC Collaborations on Advanced Reactor Licensing

In July 2013, the DOE and NRC established a joint initiative to address a key portion of the licensing framework essential to advanced (non-LWR) technologies. The initiative addressed the "General Design Criteria for Nuclear Power Plants," Appendix A to 10 Code of Federal Regulations (CFR) 50, which were developed primarily for light water LWRs, specific to the needs of advanced reactor design and licensing. The need for General Design Criteria (GDC) clarifications in non-LWR applications has been consistently identified as a concern by the industry and varied stakeholders, and was acknowledged by the NRC staff in their 2012 Report to Congress [NRC 2012] as an area for enhancement.

The initiative to adapt GDC requirements for non-light water advanced reactor applications is being conducted in two phases. Phase 1, managed by DOE, consisted of reviews, analyses and evaluations resulting in recommendations and deliverables to NRC as input for NRC staff for development of regulatory guidance. Idaho National Laboratory (INL) prepared the Phase 1 report [INL 2014] using technical and reactor technology stakeholder inputs coupled with analysis and evaluations provided by a team of knowledgeable DOE national laboratory personnel with input from individual industry licensing consultants. The DOE national laboratory team reviewed six different classes of emerging commercial reactor technologies against 10CFR50 Appendix A GDC requirements and proposed guidance for their adapted use in non-LWR applications. A set of draft Advanced Reactor Design Criteria (ARDC) was proposed for consideration by the NRC in the establishment of guidance for use by non-LWR designers and NRC staff. The proposed criteria were developed to preserve the underlying safety bases expressed by the original GDC, and recognizing that advanced reactors may take advantage of various new passive and inherent safety features different from those associated with LWRs.

Phase 2 of this initiative is managed by the NRC. In response to the Phase 1 report, NRC has published Draft Regulatory Guide DG-1330, "Guidance for Developing Principle Design Criteria for Non-Light Water Reactors" [NRC 2017]. This draft regulatory guide also describes NRC's proposed guidance for modifying and supplementing the GDC to develop Principle Design Criteria (PDC) that address two specific non-LWR design concepts; sodium-cooled fast reactors, and modular HTGRs.

The NRC has also published a policy issue for information on the subject "Accident Source Terms and Siting for Small Modular Reactors and Non-Light Water Reactors" [NRC 2016]. This report addresses the need for the NRC staff to consider mechanistic source term (MST) analysis

methods used by future applicants to demonstrate the ability of enhanced safety features of plant designs to mitigate radionuclide releases during postulated accidents, and allow future applicants to consider reduced distances to Exclusion Area Boundaries (EABs), Low Population Zones (LPZs), and population centers.

The DOE and NRC have also been jointly sponsoring workshops on advanced (non-LWR) reactors. These workshops are open to the public and provide updates on the ongoing collaborations between DOE and NRC, and also include presentations from vendors, utilities, industry organizations, and other interested parties. Workshops were held September 1-2, 2015, June 7-8, 2016, and April 25-26, 2017. Presentation materials from these workshops are available from the NRC website.

MDP-MMR Licensing Approach

The NGNP project experience provides a good model for the MDP-MMR licensing approach in the U.S. This approach will address the feedback provided by the NRC and improvements in advanced reactor licensing requirements that result from the ongoing collaboration between the DOE and NRC.

The MDP-MMR can provide a low-risk opportunity in the U.S. to evaluate an advanced reactor licensing framework that includes the RIPP approach with mechanistic source terms. MDP-MMR design features that lower licensing (and investment) risk include the low 15 MW thermal power level (and associated lower radionuclide inventory) and relatively low primary helium coolant outlet temperature (630°C) and operating pressure (3 MPa) relative to larger-scale modular HTGRs. Obtaining an NRC Design Certification for the MDP-MMR would be an important step for establishing larger-scale commercial deployment, including export markets with persistently high fossil-fuel costs that are more economically viable for nuclear deployment. This Design Certification could also provide a model for licensing larger-scale advanced reactors with similar design approaches to safety.

References

- [INL 2009] "NGNP Licensing Plan," PLN-3202, Rev. 0, Idaho National Laboratory, Idaho Falls, ID, June 2009.
- [INL 2014] "Guidance for Developing Principal Design Criteria for Advanced (Non-Light Water) Reactors," INL/EXT-14-31179, Rev. 1, Idaho National Laboratory, Idaho Falls, ID, December 2014.

[INL 2016] "Technical Program Plan for INL Advanced Reactor Technologies Technology Development Office/Advanced Gas Reactor Fuel Development and Qualification Program," PLN-3636, Rev. 5, Idaho National Laboratory, Idaho Falls, ID, May 2016.

[NGNP 2011] "Conceptual Design Report – Steam Cycle Modular Helium Reactor (SC-MHR) Demonstration Plant," NGNP-R00016, Rev. 1, General Atomics, San Diego, CA, July 2011.

[NRC 2012] "NRC Report to Congress: Advanced Reactor Licensing," August 2012, ML12153A014.

[NRC 2014] "Next Generation Nuclear Plant – Assessment of Key Licensing Issues," letter from Glenn M. Tracy (NRC) to John E. Kelly (DOE), U.S. Nuclear Regulatory Commission, July 17, 2014.

[NRC 2016] "Accident Source Terms and Siting for Small Modular Reactors and Non-Light Water Reactors", SECY-16-0012, U.S. Nuclear Regulatory Commission, February 7, 2016.

[NRC 2017] "Draft Regulatory Guide DG-1330, Guidance for Developing Principle Design Criteria for Non-Light Water Reactors," U.S. Nuclear Regulatory Commission, February 2017.